TÉCNICO LISBOA

Comparative Study of Solar Cell Technologies

Afonso Pedro Nunes da Silva Ravasco

Thesis to obtain the Master of Science Degree in

Electrical and Computer Engineering

Supervisor: Prof. João Paulo Neto Torres

Examination Committee

Chairperson: Prof. Francisco André Corrêa Alegria
Supervisor: Prof. João Paulo Neto Torres
Member of the Committee: Prof. António Carlos De Campos Simões Baptista

November 2021

I declare that this document is an original work of my own authorship and that it fulfills all the requirements of the Code of Conduct and Good Practices of the Universidade de Lisboa.

Declaro que o presente documento e um trabalho original da minha autoria e que cumpre todos os requisitos do Código de Conduta e Boas Práticas da Universidade de Lisboa.

Agradecimentos

Em primeiro lugar quero agradecer a todos os meus amigos que me acompanharam toda esta joranada que tem sido este curso.

Quero agradecer ao meu orientador, o Professor João Torres por me ter guiado não só durante todo este período da elaboração da tese e do IIEEC, mas também por ser um grande professor que está sempre lá para apoiar os seus alunos. Foi sempre uma grande inspiração e é com muito gosto e orgulho que digo que foi ótimo trabalhar consigo!

De seguida, a próxima pessoa da qual eu pude contar sempre para tirar as dúvidas que precisasse e que me colocou sempre à vontade foi o grande Ricardo Lameirinhas. Obrigado pela tua ajuda e dicas não só durante a tese, mas também durante todo o curso!

Um obrigado também à minha família que me sempre apoiou durante todo estes anos, sobretudo aos meus pais, precisamente pelo vosso carinho e por me terem dado esta oportunidade de poder seguir os meus sonhos. Estarei sempre grato a vocês por me terem acompanhado e por me fazerem o homem que sou hoje, espero que vos tenha trazido orgulho.

Ao ínicio, esta viagem foi um pouco mais dura do que tinha pensado, mas houve alguém que fez com que o caminho turtuoso que se encontrava à minha frente, fosse sempre mais fácil de lidar. Obrigado por todo o teu apoio, amor e boa disposição para me levantares nos dias maus e melhorares os bons dias. Obrigado Ana!

Por fim, gostaria de fazer um agradecimento especial ao meu parceiro de noitadas que teve sempre comigo a dar-me apoio moral durante as noites intensas de trabalho. A very good boy, Kiko.

Abstract

When you think about sustainable energy, the first one that comes to mind is always solar power. It is amazing to think that photovoltaic (PV) technologies have been around for more than 70 years and it has evolved from just a small scientific research paper to a million dollar market.

Throughout these whole 70 years, many materials have been subjected into tests and experiments, creating several photovoltaic generations. In this work, some of these generations will be compared with one another, in order to see what were the significant changes, not only in the material, but what do these materials contribute to for the photovoltaic community. To better study these materials, a 2D solar cell PIN model was developed using the software *COMSOL Multiphysics*. The designed model was produced with an electrical approach in mind, where its features such as the doping of the semiconductor and the incident wavelength can be user-defined.

In addition, experimental tests were also adopted, in order to have real case scenario of the types of solar panels at hand as well as a SEM analysis of the same solar panels, to obtain a better understanding of the internal layers.

Keywords

Photovoltaic Technology; Solar Cells; Silicon; CIGS; photovoltaic devices.

Resumo

Quando ouvimos falar sobre energias sustentáveis, o primeiro termo que vem à mente é energia solar. É bastante impressionante quando olhamos para a evolução da tecnologia fotovoltaica e reparamos que já passaram mais de 70 anos desde a criação da primeira célula solar, evoluindo de um pequeno artigo científico para um mercado de milhões de euros.

Ao longo destes 70 anos, muitos materiais foram sujeitos a testes e experiências, originando várias gerações de tecnologia fotovoltaica. Neste estudo, algumas destas gerações vão ser comparadas e analisadas, de modo a verificar possíveis alterações, não só ao nível dos materiais, mas na contribuição que estes materiais dispõem para a comunidade fotovoltaica. Para ter uma melhor percepção, um modelo 2D de uma célula solar tipo PIN foi desenvolvida usando o software *COMSOL Multiphysics*. O modelo projetado foi produzido tendo em conta uma abordagem elétrica da célula, onde certas caraterísticas do material semicondutor podem ser definidas, como a dopagem e o comprimento de onda da radiação incidente.

Foram também realizados alguns testes experimentais, de modo a poder obter um cenário real de diferentes tipos de paineis solares de diferentes tecnologias, assim como uma análise SEM dos mesmos paineis, com o objetivo de compreender de forma mais aprofundada as camadas internas dos mesmos materiais.

Palavras-chave

Tecnologias Fotovoltaicas; Células Solares; Sílicio; CIGS; Dispositivos fotovoltaicos.

Contents

List of Figures

List of Tables

Acronyms

CIGS - Copper Indium Gallium Selenide

PV - Photovoltaic

FF - Fill Factor

PSC - Perovskite Solar Cell

OSC - Organic Solar Cell

DSSC - Dye-sensitized Solar Cell

c-Si - Crystalline Silicon

mono-Si - Monocrystalline Silicon

poly-Si - Polycrystalline Silicon

a-Si - Amorphous Silicon

PCE - Power Conversion Efficiency

CdTe - Cadmium Telluride

TCO - Transparent Conductive Oxide

Mo - Molybdenum

FTO - Flourine-doped Tin Oxide

TiO_2 - Titanium Dioxide

R2R - Roll-to-Roll

WEEE - Waste Electrical and Electronic Equipment

HGMS - High Gradient Magnetic Sepration

GaAs - Gallium Arsenide

CIS - Copper Indium Selenide

CGS - Copper Gallium Selenide

UV - Ultra-violet

IR - Infra-red

SEM - Scanning electron Microscope

EDS - Energy-Dispersive analasys

Chapter 1: Introduction

1.1 Motivation

Solar technology has came a long way since the design of the first crystalline silicon solar cell back in 1954 in the Bell Laboratories, USA, registering an efficiency of about 4%. Nowadays, crystalline silicon solar cells are able to produce efficiencies above 25% and the continuous research of solar cells allowed the creation of thin-film solar cells and later the first solar cell made purely of organic materials, each of them marking different generations within the history of PV technology.[5]

There are mainly two materials that are going to be subjected under analysis in this study: CIGS and silicon. Silicon, representing the 1st generation of solar cells, is known for its market domination and to be the top material in solar panel production. It is known to produce very high efficiencies and have a wide absorption range. CIGS, on the other hand, is representing the 2nd generation, specifically the thin-film technology. Thin-films are known to use much less material than other solar cells and recently have achieved promising results. However, some of the CIGS cells contain toxic elements (such as Cadmium) that limit the commercial production, but which benefits their efficiency. Nonetheless there are other types of CIGS that can be cadmium free, but haven't reached a efficiency as high as the cadmium CIGS cells.[15]

Some other materials were taken into consideration as well. During the simulation, Gallium Arsenide (GaAs) was also considered as well as dye-sensitzed solar cells (DSSC) in the experimental process. DSSCs were used in this work to represent the 3rd generation, however as it will be shown later DSSCs could not be used in some of the components of the study.

1.2 Main objectives

During this study, the creation of a 2D model of a solar cell was set to be the main goal. The model to be used was defined to be an approximation of an actual solar cell, mainly focused on the absorber layer, responsible for generating electron-hole pairs. This model was designed with the *COMSOL Multiphysics* software and originally the 2D model was based on a sample module of a Gallium Arsenide PIN photodiode which was later altered to fit the goal of the study.

Another goal of the model was defining parameters of the solar cell and the radiation. If the user wanted to change the solar cell at hand, it was possible to change the material or the type of doping that was wanted, as well as the frequency of the incident radiation.

The materials under analysis are mainly CIGS and silicon, but in some cases other materials are considered, such as the GaAs and the dye-sensitized solar cells.

Lastly, real case scenarios will also be taken into consideration, in order to study the materials more extensively. To complement this experimental component, a SEM analysis will be used as well, mainly to determine the inside layers of the studied materials.

1.3 Outline

On chapter 2, the theoretical foundations will be set. A brief explanation of the solar cell and the basic principles of p-n junctions will be addressed, as well as some metrics that will later be used to determine the performance of a solar cell, followed by some of the equations and principles that were used under the simulation of the 2D model.

Following the theoretical foundations, chapter 3 is entered. Here, the state-of-art of the solar cell technologies will be discussed, focusing firstly on the evolution of the solar cell materials, followed by some applications, as well as their industrial production. It is also important to factor in the recyclability of each of the materials at hand, since nowadays this is a very big hot topic and requirements for the reduction of photovoltaic waste must be in order.

Afterwards, the focus converges on the designed 2D PIN model of the solar cell. Here, the main topics of discussion will be the simulations that were conducted using this very model. The responsivity and the Current-Power relation were the main simulations to be executed. The main materials that were used were silicon, Gallium Arsenide (GaAs) and CIGS.

Chapter 5 will be directed at the experimental results for different types of solar panels. Here 3 solar panels will be tested in order to obtain their I(V) characteristic as well as their efficiency and fill factor. In the end there will also be a comparison between the emission spectrum of the light bulb that was used, with the simulated responsivity of each material, as well as a calculation of the V_{OC} according to it's band gap.

Finally in Chapter 6, a SEM analysis was conducted in order to better understand the constitution of the solar panels that were used in the previous chapter. This could justify any deviations from the obtained results and to better understand the constitution of the solar cell.

In the final chapter, a general overview of the obtained results is going to be used discussed, followed by a few comments on future work to be done in this topic.

Chapter 2: Theoretical Foundations

2.1 Electrical properties of a p-n junction

The p-n junction is commonly used for solar cells. This junction creates a charge separation of electron and holes and when the junction is formed, the large carrier concentration gradients cause the diffusion of carriers, i.e., holes diffuse from p-type semiconductors to n-type semiconductors and electrons diffuse from the way around. Because of the ionized impurity atoms, a layer without mobile charge carriers is formed when the electrons and holes diffuse across the junction, hence creating an electric field in this area which is called the depletion region.[4][44].

Once the drift current is balanced by the diffusion the thermal equilibrium is established. At this point, the Fermi levels of the p-type semiconductor and n-type semiconductor are equal as it can be seen in Figure 2.1.

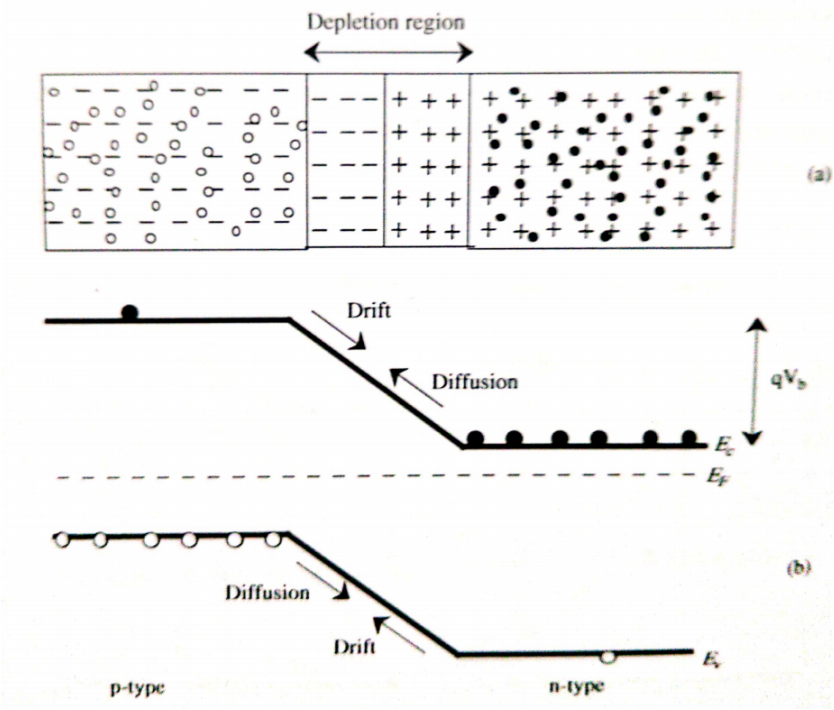

Figure 2.1: a) Schematic structures of a p-n junction b) Its energy band diagram in thermal equilibrium.[44]

2.2 p-n junctions as solar cells

A solar cell or a photovoltaic cell (PV cell) is the main responsible for solar irradiance conversion into electrical energy. It is composed by a simple p-n junction like a diode. Despite, diodes being passive components that emit light once subjected to an electrical current, the PV cell behaves very differently once it is under light. The p-n junction has a photoconductive behaviour, to which its called photodiode.

The Photodiode can be either a passive or active device, which respectively translates into a photoreceptor and a PV cell. The I(V) curve of the PV cell under no source of light, behaves exactly as a diode, but once it is illuminated

it sparks an offset in the current, as it can be seen in Figure 2.2. This current is called the photogenerated current I_L, created by the generation of eletron-hole pairs due to the incident light. This current is proportional to the light intensity. [26]

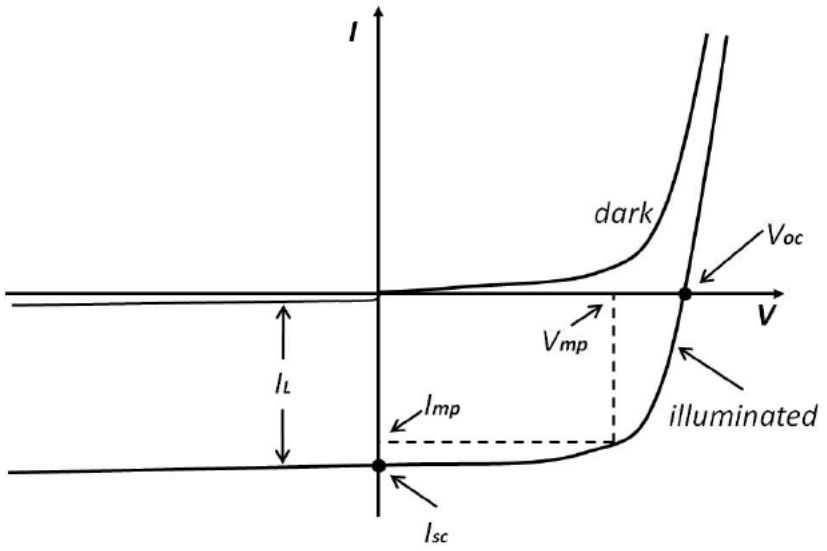

Figure 2.2: I(V) curve of a solar cell. [26]

$$I(V) = I_s(e^{\frac{V}{nV_t}} - 1) - I_L \tag{2.1}$$

Given the previous equation, an ideal model of a PV cell's equivalent circuit can be given by the Figure 2.3. In this Figure, it is possible to observe the representation of the p-n junction through the ideal diode and the external light source given by the current source, I_L. [26][44]

Once again in Figure 2.2 it is possible to point out the produced curve under illumination is shifted by a factor of I_L. This value of I_L can be better perceived as the short-circuit current, I_{SC}, since it is the generated current for a zero input voltage. Another important point in this curve is the V_{OC} voltage, which denotes the instant where the PV cell's current reaches zero, hence the denomination open-circuit voltage. These two values are very important, since the play a major role in the definition of the solar cell's I(V) characteristic. [44] On a side note, Equation 2.1 is usually the way current-voltage curves behave. However, to be more convenient, the I(V) curve of the solar cell is plotted on the 1^{st} quadrant, changing only the sign of the current. With this statement in mind, it's possible to rewrite the expression as:

$$I = I_L - I_s(e^{\frac{V}{nV_t}} - 1) \tag{2.2}$$

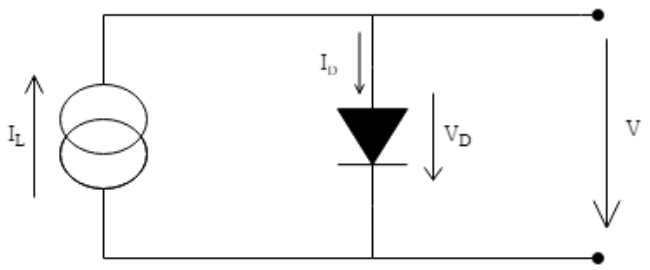

Figure 2.3: Solar cell, ideal circuit

Through this equation it's possible to obtain the short-circuit current, I_{SC}, which is given by,

$$I_{SC} = I_L, for V = 0 \tag{2.3}$$

And the open circuit voltage is described as the following,

$$V_{OC} = \frac{kT}{q} ln(1 + \frac{I_L}{I_s}) \tag{2.4}$$

Equation 2.4 shows that V_{OC} depends on the saturation current of the solar cell and the light-generated current. In the next chapters of this thesis, the relationship of V_{OC} with the E_g will be shown, mainly due to the dependency on the saturation current.

However, it is possible to notice that the open circuit voltage depends on the temperature of the cell. At a first glance, one might say that the V_{OC} increases linearly with temperature. This is not true. I_0 increases at a very fast pace with temperature, which influences the logarithm, thus decreasing the V_{OC}

Another parameter of the solar cell, as it was seen is the short-circuit current. For an ideal solar cell, Equation 2.3, is true. Nonetheless, this current usually depends on several factors. One of them is the area of the solar cell, and usually to remove this dependence, it is used the short-circuit current density, J_{SC}, given by Equation 2.5.

$$J_{SC} = \frac{I_{SC}}{A} \tag{2.5}$$

The I_{SC} also depends on the number of photons (or the incident power of the light source). The short-circuit current is directly dependant (linearly) on the light intensity. Other factors like, the optical properties and the spectrum of the incident light also play a huge role on the definition of the I_{SC}.

However, solar cells contain certain defects that prohibits them to be ideal. For instance, the resistance (R_s) along the copper wiring of the PV cell plays a major role in the shape of the I(V) curve, which is usually depicted as a resistor in series with the cell at hand. There is also another type of influence due to any current leakage, which is certain fractions of current are loss to ground, usually depicted as a parallel resistance to the cell called the *shunt* resistance (R_{sh}).

$$I = I_L - I_{is}(e^{\frac{q(I \cdot R_s + V}{nkT}} - 1) - \frac{I \cdot R_s + V}{R_{sh}} \tag{2.6}$$

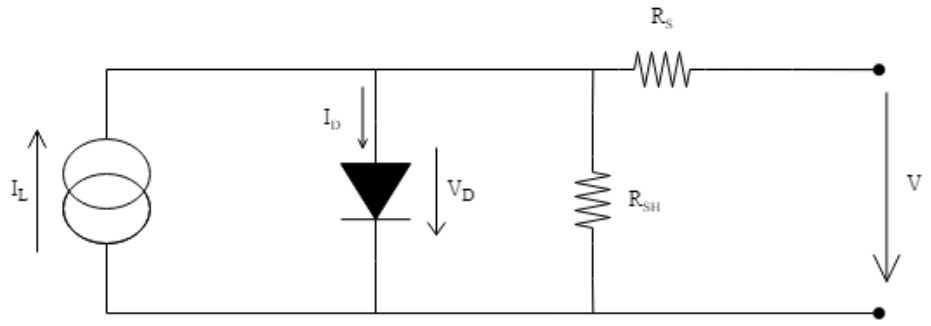

Figure 2.4: Real solar cell, depicted by the current leakage and copper losses

The series resistance affects mostly the I_SC, as it is possible to see in Figure **??**, different values of R_s and the different shapes of the I(V) curve.

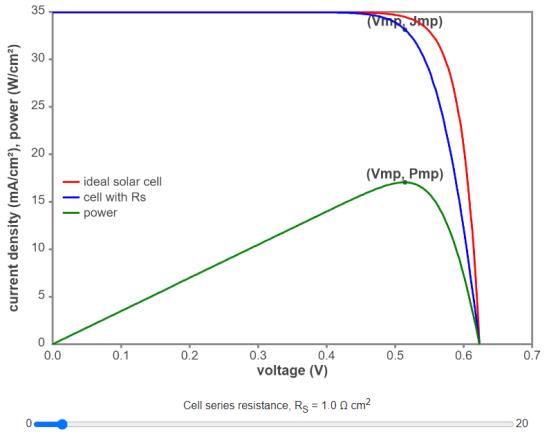

(a) I(V) curve for $R_s = 1.0\Omega cm^2$

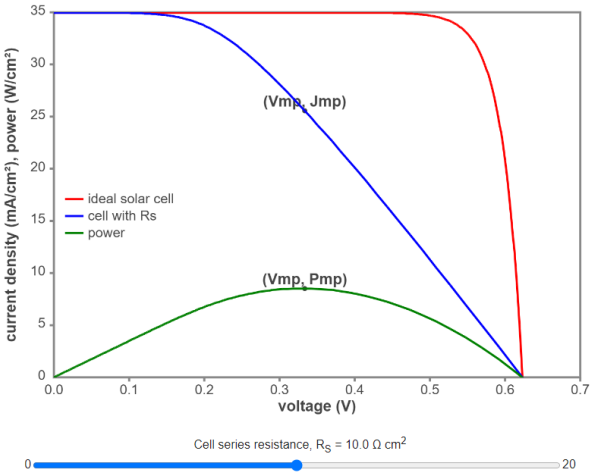

(b) I(V) curve for $R_s = 10.0\Omega cm^2$

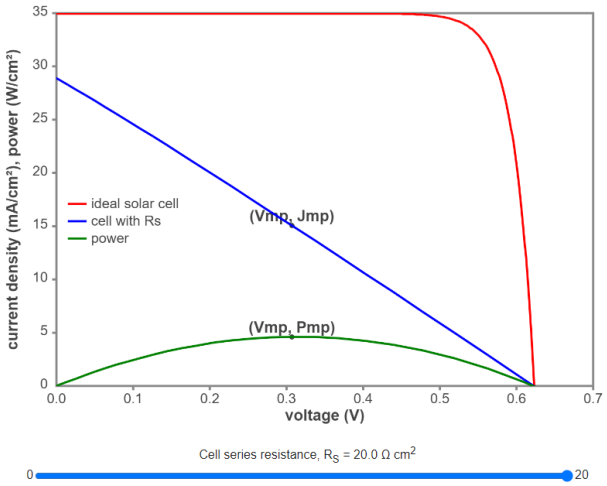

(c) I(V) curve for $R_s = 20.0\Omega cm^2$

Figure 2.5: Different I(V) curves for different values of R_s, using the series resistance simulator.[42]

The series resistance affects mostly the I_SC, as it is possible to see in Figure 2.5, different values of R_s and the different shapes of the I(V) curve, especially in the latter parts of the function.

In addition to the series resistance, the shunt resistance also has a negative impact on the I(V) curve of the solar cell, as it can be seen in Figure 2.6. The I_{SC}, although it remain partially unchanged, it's the V_{OC} that is penalized.

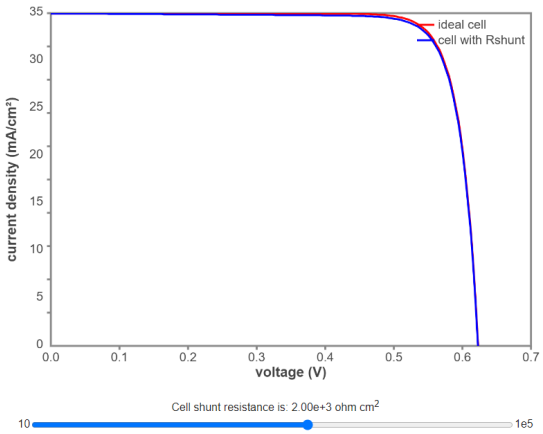

(a) I(V) curve for $R_{sh} = 2.0k\Omega cm^2$

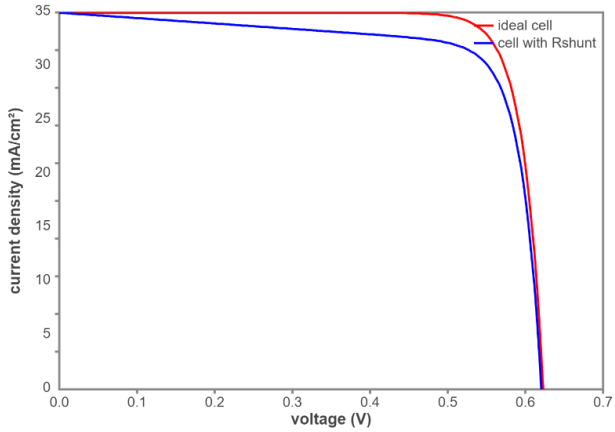

(b) I(V) curve for $R_{sh} = 200.0\Omega cm^2$

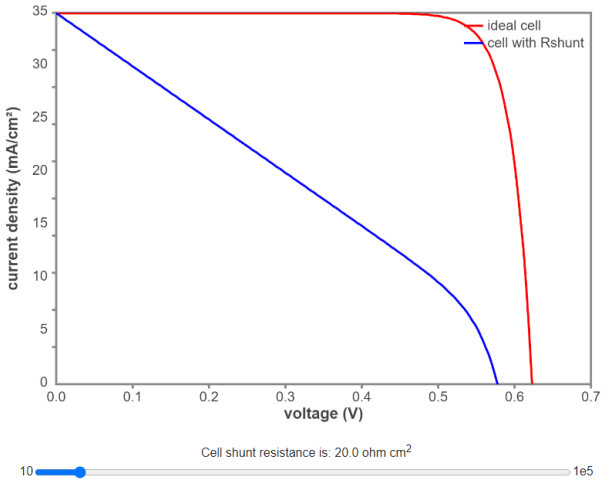

(c) I(V) curve for $R_{sh} = 20.0\Omega cm^2$

Figure 2.6: Different I(V) curves for different values of R_{sh}, using the series resistance simulator.[43]

The short-circuit current and the open-circuit voltage are the main corner cases of current and voltage of the solar cell, since at both of these operating points, the power from the solar cell is zero. The fill factor (FF) is the parameter used to measure the quality of the solar cell, determining the maximum power from a solar cell in conjunction with the V_{OC} and the I_{SC}, determining how close the solar cell is from its ideal model. Mathematically, the FF is given as the ratio of maximum power from the solar cell with the product of V_{OC} and I_{SC} (Equation 2.7), which in theory would correspond to the highest power possible for a solar cell to produce [18]. The typical values for the FF are around the 0.6 and 0.8 mark, the closer to 1 the better, because the cell can provide more power.

$$FF = \frac{P_{Max}}{V_{OC} \cdot I_{SC}} = \frac{V_{MaxPower} \cdot I_{MaxPower}}{V_{OC} \cdot I_{SC}} \tag{2.7}$$

However, the FF can be seen as the measurement of "squareness" of the I(V) curve, from a graphical point of view, or it can be seen as the ratio of the rectangular areas depicted in Figure 2.7. The FF is mainly influenced by the parasitic resistances, R_s and R_{sh}, since they affect the "squareness" shape of the curve, but from an electrical point of view they reduce the maximum voltage and current points. [18]

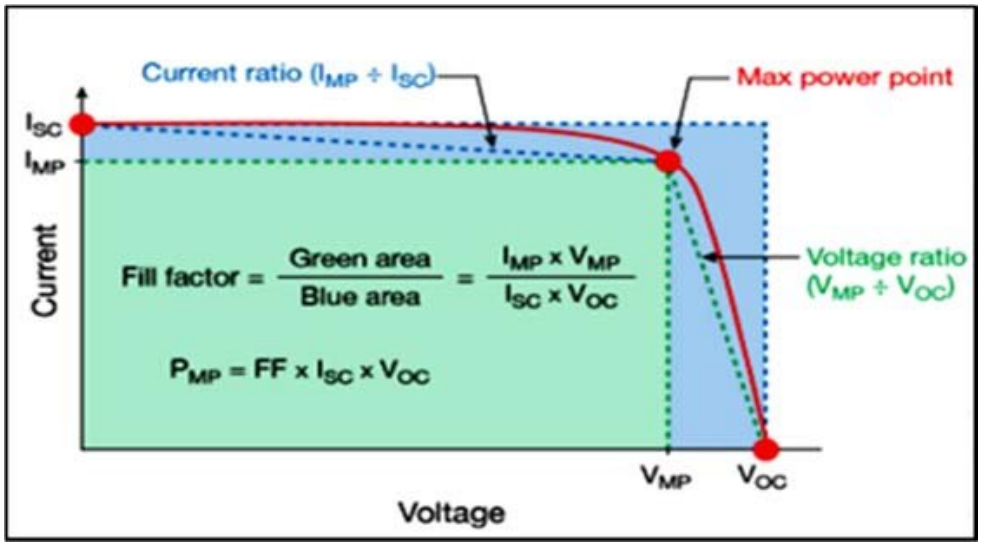

Figure 2.7: Fill factor depiction on an I(V) curve.[2]

The efficiency of a solar cell is the most commonly used parameter to evaluate its the performance. It is defined as the ratio of output energy from the solar cell to input energy from the incident radiation.

$$\eta = \frac{V_{OC} \cdot I_{SC} \cdot FF}{P_{in}} \tag{2.8}$$

2.3 Equations used in the model

In this section, the equations that were used in the *COMSOL Multiphysics* model are going to be broken down. Since it was used two modules to design the solar cell, this section will divide into the semiconductor module, responsible for defining the material properties of the solar cell, and the electromagnetic waves module, responsible for generating the incident light onto the solar cell.

2.3.1 Semiconductor module

Firstly, the semiconductor material model is used and this model is the central node of the semiconductor module, since it defines the basic principles of the semiconductor. The main parameters of the semiconductor are defined in this section, such as the relative permittivity, the electron affinity, band gap and so on. The basic equations that operate in this region are the equations related to the definition of the conduction and valence bands (Equation 2.10 and 2.11 respectively), the current density of electrons and holes (Equations 2.12 and 2.13, respectively) and the semiconductor's charge density (Equation 2.9).

$$\rho = q(p - n + N_d^+ - N_a^-) \tag{2.9}$$

$$E_c = -(V + \chi_0) \tag{2.10}$$

$$E_v = -(V + \chi_0 + E_{g,0}) \tag{2.11}$$

$$J_n = qn\mu_n \nabla E_c + \mu_n k_B T G(n/N_c)\nabla n + qnD_n \nabla \ln(T) \tag{2.12}$$

$$J_p = qp\mu_p \nabla E_v + \mu_n k_B T G(p/N_v)\nabla p + qpD_p \nabla \ln(T) \tag{2.13}$$

Where, the k_B is the Boltzmann constant, G is the Generation rate. D_n and D_p are the drift diffusion coefficients of electron and hole respectively.

The next step to be considered in the model is the doping. There are two types of doping.

The analytic doping density allows the user to specify in a block-shaped region the doping to be defined, along with the decay profile away from the region, approximating it to a diffusion process. The decay of the dopant is defined by the specification of a junction depth, d_j, given by the following equations.

$$N_{A,D} = N_{A,D}^{user} \tag{2.14}$$

$$N_{D,A} = N_{D,A}^{user} + N_{D0,A0} \exp\left(-\left[\left(\frac{r_x^-}{l_x}\right)^2 + \left(\frac{r_x^+}{l_x}\right)^2 + \left(\frac{r_y^-}{l_y}\right)^2 + \left(\frac{r_y^+}{l_y}\right)^2\right]\right) \tag{2.15}$$

$$l_x = l_y = \frac{d_j}{\sqrt{\ln\left(\left|\frac{N_{A0}}{N_b}\right|\right)}} \tag{2.16}$$

If the region is n-doped, then the first index of the equation should be considered (acceptors), but if a p-doped region is preferred then the second index of the equations is used (donors). Also, r_x and r_y are the base position where the diffusion will start.

This type of doping is the one used to define the p-doped layer and the n-doped layer, later in the model (Chapter 4).

On the other hand, there is also the geometric doping model, which works in parallel with the analytic model. This enables the doping profiles to be expressed as a function of distance from selected boundaries. The junction depth is applied here as well and it specifies the distance from the selected boundaries at which the dopant concentration is equal to the specified background doping. In other words, this doping model dopes the boundary of the semiconductor all the way until the junction depth, hence creating the p+ doping contact and the n+ doping contact in the model.

2.3.2 Electromagnetic Waves module

The Electromagnetic Waves module was also used in the model to recreate the incident radiation. The following equations represent how the electric field is calculated for every point in the domain (solar cell).

$$\nabla \times (\nabla \times \mathbf{E}) - k_0^2 \epsilon_r \mathbf{E} = \mathbf{0} \tag{2.17}$$

Given that, ϵ_r

$$\epsilon_r = (n - ik)^2 \tag{2.18}$$

Where, n and k are respectively, the real and imaginary part of the refractive index.

$$\mathbf{E}(x, y, z) = (x, y)e^{-ik_z z} \tag{2.19}$$

Where, k_z is the wave's propagation constant.

Chapter 3: Evolution of Solar Cell Materials

3.1 Solar Cell Technological Tree

The Solar cell technology has been evolving over the last 50 years. There have been many different types of photovoltaic devices and technologies throughout the years, so to sort out these technologies, they have been inserted into generations, according to the properties of their materials and evolution of time as well.

The most common solar cells available in the market belong to the first-generation, the single band-gap solar cells, comprised by germanium and the most dominating material in the PV market, silicon. Silicon is one of the most abundant materials on Earth, accounting about 25% of its crust, as well as being very cheap and it's easily producible.[36]

The second-generation is based on thin film technologies. This technology was introduced to reduce the material usage from the previous solar cells, achieving layers as thin as tens of micrometers or even nanometers. This layer is deposited on a layer of substrate such as glass, stainless steel or plastic and due to the thinness of this layer it is possible to build flexible devices that can have many different applications. Some examples of second-generation materials are amorphous silicon, gallium arsenide and copper indium gallium diselenide (CIGS) [38].

There is also the third-generation, which includes the non-based silicon solar cell materials, such as perovskite solar cells (PSC), organic solar cells (OSC) and dye-sensitized solar cells (DSSC). These types of photovoltaic technology use a combination of organic and inorganic materials to generate electron-hole pairs, hence creating a photovoltaic effect throughout several layers. Despite some of these cells still struggle to provide a good efficiency, significant progress on the power conversion efficiency (PCE) of these cells is being made, guaranteeing a promising future for this technology. [1][44]

3.1.1 1st Generation - Silicon

The first semiconductor-based solar cells with energy-conversion efficiencies larger than 10% were made of silicon, during the 1950s and 1960s. At present, 85-90% of the solar PV modules are produced worldwide are based on crystalline silicon (c-Si) wafers, a $160 - 240\mu m$ thick slice, cut from a single silicon ingot.[9] [44] There are two main types of c-Si:

- Monocrystalline silicon
- Polycrystalline silicon
- Ribbon and sheet-defined film growth

Monocrystalline cells are created from manufactured wafers through expensive single-crystal growth methods, in order to produce a higher quality silicon ingot. The record for monocrystalline solar cells in a laboratory is 25.6%, however for commercial use the efficiency comes around 17-20%.[11]

Polycrystalline cells are formed from multicrystalline wafers assembled from a cheaper cast solidification process and much less expensive to produce, resulting in a more affordable end price for the consumer. Consequently polycrystalline cells are marginally less efficient, with an average conversion efficiency around 14-16%.[35][9]

Ribbon and sheet-grown silicon doesn't require any slicing from ingots, but it uses molten silicon to perform a typical procedure in crystals called epitaxy. Epitaxy is a type of material deposition in which new orientated crystalline layers are formed with respect to a substrate layer (seed layer)[32]. A crystalline film of molten silicon is deposited on top of a seed layer of monocrystaline silicon. These processes can be considerably cheaper, as there is no material waste from wafer slicing, achieving cells with a maximum efficiency of 21%.[9]

(a) Silicon monocrystalline solar cell. [34]

(b) Silicon polycrystalline solar cell. [34]

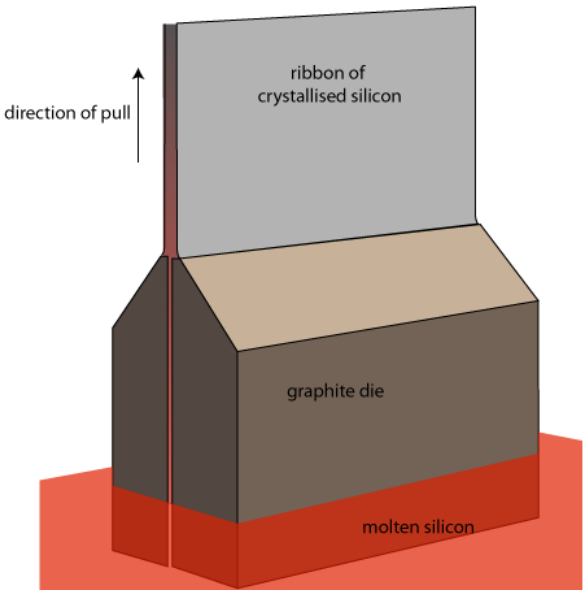

(c) Production of ribbon crystallised silicon solar cell [50].

Figure 3.1: Different types of c-Si solar cells.

Nowadays, Silicon still remains the most common 1st generation material to be used in PV panels to this day. Thin-film solar cells were later introduced and marked the beginning of the 2nd generation, however, silicon evolved itself into the 2nd generation as well, all due to amorphous silicon (a-Si). In this study, a-Si won't be focused but

it's important to recognize that there are still a lot of studies under analysis about possible upgrades for the silicon material.

3.1.2 2nd Generation - CIGS

The 2nd generation of PV technology was marked by the creation of thin-film photovoltaics. Although the main majority of the market is withhold by the silicon industry, the rest of the market share is detained by the thin-film PV. CdTe, CIGS, amorphous and thin-silicon have been the main dominating materials in this generation. These materials produce solar cells at the micrometer scale, introducing the possibility of developing light weight and versatile pv panels, increasing the possibilities of newer applications [39].

The other game changing feature, later incorporated into the thin-film industry, was the possibility to create flexible solar cells. This not only can potentially maximize the energy production area, but also allows the thin-film cells to be produced in roll-to-roll industrialization, which can facilitate the production to a large-scale extent. [15]

A thin-film CIGS solar cell is commonly composed by 7 layers with different materials:

- **Substrate** - Usually made of glass, however can be made from another material depending on the use case (e.g. flexibility);
- **Back Contact** - Molybdenum, also known as Mo;
- **Absorber layer** - CIGS material;
- **Buffer layer** - Cadmium Sulphide (Cds) or Zinc Oxy Sulphide (Zn(O, S));
- **Window Layer** - high resistive undoped Zinc Oxide (i-ZnO);
- **TCO Layer** - Aluminium doped Zinc Oxide(ZnO:Al)

Nowadays, the most commonly used **substrate** is soda-lime glass, since it gives the CIGS cell more stability. The substrate can either be produced from a rigid or flexible material, but the flexible substrates cannot handle temperatures above 500^{o}C, so to fabricate flexible CIGS solar cells, a low temperature procedure must be adopted. Nevertheless, rigid CIGS cells use soda-lime glass, not only because it can withstand the desired high temperatures of fabrication, but also because of the high amount of sodium which is beneficial to increase the open-circuit voltage and Fill Factor of the cell, hence achieving higher efficiencies. Despite bringing a lot of value into the CIGS cell, a good substrate must not allow impurities to diffuse into the other layers, making the sodium the only exception to this rule of thumb.

After the substrate, there is the **back contact**, composed of molybdenum (Mo). This material collects and stores the charge carriers that were generated by the absorber layer and separated at the p-n junction. Mo is the preferred material for the back contact, because Mo and CIGS do not heavily react together and is more chemically and mechanically stable during the selenization operation, thus creating a thin layer of molybdenum selenide ($MoSe_2$) at the CIGS/Mo interface. The back contact, must also enable the diffusion of sodium from the rigid substrate into the CIGS absorber layer [37].

The **absorber layer** is the main layer of the solar cell, since it is composed by the copper indium gallium diselenide, $Cu(In_{1-x}, Ga_x)Se_2$, represented in Figure 3.2. The CIGS material is a p-type polycristalline semiconductor with a direct band gap and a high optical absorption coefficient and is presented in the absorber layer since it is where the electron-hole pairs are generated. The composition of this region is very crucial to the performance of the cell at hand, because the ratio of Ga and In determines all the electronic band structure of the cell. According to the literature, for $CuInSe_2$

(CIS) the band gap is $1.04eV$ and for $CuGaSe_2$ (CGS) is $1.67eV$, thus the the higher the band gap the higher the Ga concentration.

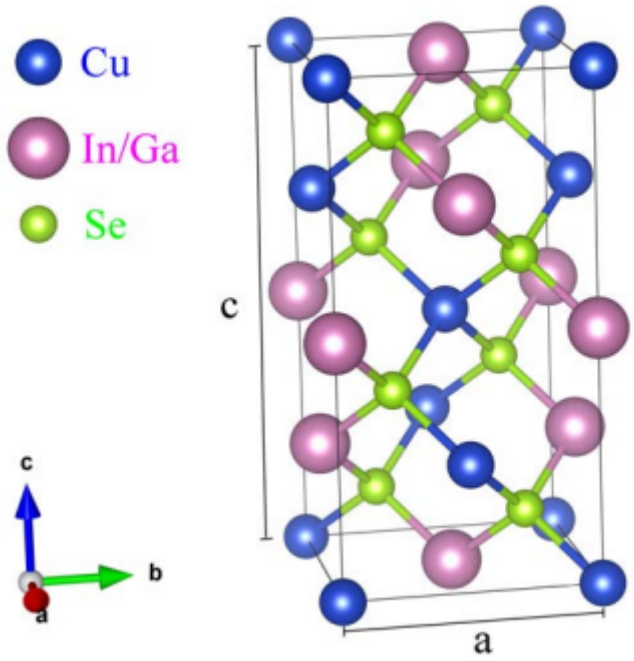

Figure 3.2: Unit cell of CIGS. Each Se atom is the center of a tetrahedral bond with two Cu and two In/Ga atoms.[25]

In addition, the **buffer layer** is the n-type layer to form the p-n junction with the p-type CIGS. The most used buffer layer is CdS since it holds the highest efficiency for the solar cell. In spite of topping the high efficiency ranks, the toxicity of cadmium and high band gap raises a few environmental issues and high absorption losses of the cell. Therefore, other materials have been explored to assume this role, such as ZnO or ZnS, which offer less absorption losses and similar electronic properties [45].

Then there is the **Transparent Conductive Oxide layer (TCO)** and the **Window Layer**. Before the deposition of the Aluminium doped Zinc Oxide on the TCO, a thin layer of intrinsic high resistive Zinc Oxide is coated to minimize the creation of shunt paths originated from the p-n junction. This window layer is dependent on the quality of the CIGS and buffer layers. The TCO's ZnO:Al is then deposited on top of the i-ZnO layer. The band is an n-type semiconductor and transparent so the light can travel to the CIGS absorber layer and it must be a conductive material to transport the electrons.

Major advances have appeared in the past years for thin-film technologies, including CIGS. For absorber layers, nowadays, there are about ten different procedures under development worldwide [46]. Standardization is also one of the main issues to be addressed as well, since it benefits immensely thin film PV manufacturing in larger scales. Thin film PVs offer a large variety of applications to pursue, including rooftop and utility-scale applications, as well as building-integrated photovoltaics (BIPV) and even space exploration, due to their high radiation resistance.

The best example of BIPV is the Building Integrated thin-film CIGS façade on the Honda building in Japan, Figure 3.3. Honda announced in 2007 its involvement in the photovoltaic industry through a subsidiary company, Honda Soltec, with the specific production of CIGS thin-film solar panels. To raise awareness to it's new product, one of the walls of the Honda Soltec headquarters was covered with Honda's CIGS PV panels, producing around 22kW of power.

Figure 3.3: Honda Soltec building in Japan, with its thin-film CIGS wall [46]

3.1.3 3rd Generation - DSSC

On the other hand, third-generation solar cells have been surfacing even more in the past years. OSC, PSC and DSSC technologies have had a vast study, increasing the power conversion efficiency (PCE) up to the 25% mark.

A DSSC is a photovoltaic device that uses an internal dye as a photo-sensitizer, acting as the solar energy absorber of the cell. A normal DSSC is composed by two conducting glass electrodes evolving some photoconductive layers in between. Firstly, there is a **fluorine-doped tin oxide (FTO)** pre-coated on to one of the external glasses to make them conductive. Right under this layer, the dye region is reached. In this region there is a small layer of **Titanium Dioxide, TiO_2**, which acts as a holding place for the dye that is mounted on the surface of the TiO_2. The main goal of the **dye** is to absorb the sunlight's photons and converting it into electrical energy, so the performance is very dependent on the the type of dye used as the sensitizer. There can be two types of dyes:

- **Inorganic dyes** - Usually these types of dye have a metal complex and are known to achieve higher PCEs, however some of these materials have proven to be very hazardous and toxic materials, as well as being very rare materials, such as Ruthenium, Ru, one of the most used dye materials in DSSC production.
- **Organic dyes** - On the other hand, the organic dyes prove to be a more sustainable approach, since they can be used natural dyes, such as extracted dyes from Raspberries, Hibiscus and Chlorophyll. Each of these materials has a different absorption spectrum, so the type of incident radiation will produce different results. There is also the prospect of producing synthesized organic dyes, but it is a complicated and costly process.

The photoexcitation of the dye will cause an injection of electrons into the conduction band of the TiO_2. These electrons are scattered through the TiO_2 nanoparticles and traverse the FTO layer (the electrode) to reach to the external load. On the other side of the dye, a liquid electrolyte is placed between the working electrode and the counter electrode. The most used electrolyte is the iodide-triiodide ($I^-/I_3{}^-$) redox system which works in balance with the TiO_2.

The DSSC works as a redox cycle and the iodide electrolyte closes this loop, as it can be seen in Figure **??**. After losing an electron, the dye remains positively charged, caused by the absorption of sunlight, generating what is called in chemistry an oxidation reaction. However, the I^- ion will quickly replace the lost electron, by donating one of its electrons. The reduction of the dye, allows the dye to return to its natural state, while producing $I_3{}^-$ ions. The I^- is regenerated to its natural form through the reduction of $I_3{}^-$ from the counter electrode, where the electrons are supplied via the external load, thus completing the cycle, without any permanent chemical transformation.

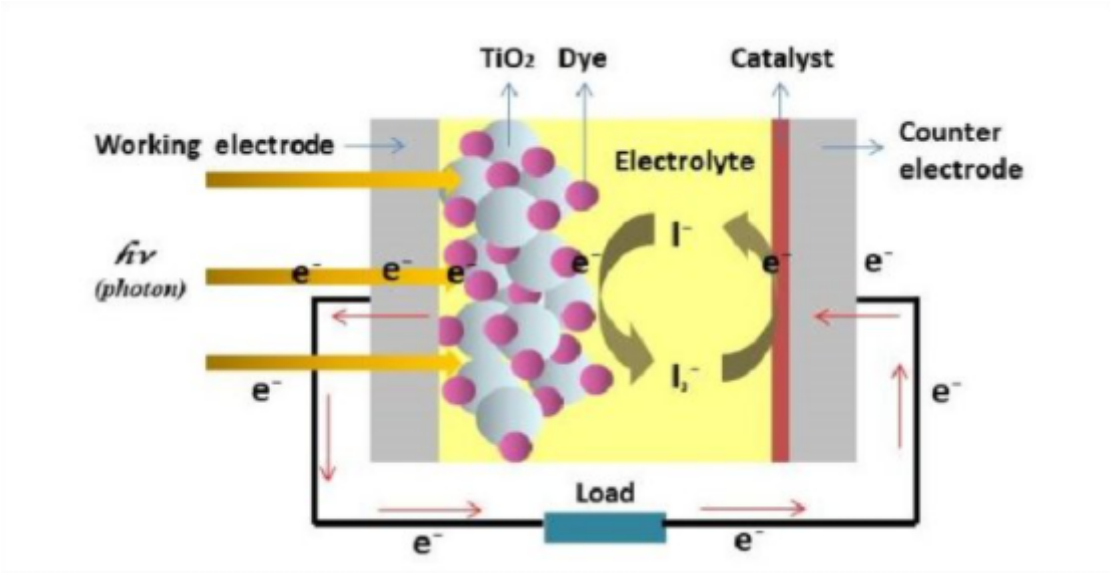

Figure 3.4: Basic structure and operating principle of DSSCs. [20]

The first DSSC ever to be assembled and tested dates back to the year 1991 by Professors Michael Grätzel and Brian O'Regan. Inspired by the principle of photosynthesis, Grätzel and O'Regan developed a DSSC with a maximum PCE of 7%. This pioneering publication sparked future investigations on this subject, marking the beginning of the 3rd generation of photovoltaic technology. Throughout the years, some companies have focused their activity on glass-based and flexible DSSC development, industrial production and marketing. The first commercial of DSSC applications have been established in small electronics and mobile device sectors, such as decorative solar lamps, flexible mobile phone chargers and solar bags [20]. The DSSC technology has shown that it has advanced from the RD stage, while other PV materials such as PSCs (high efficiency) and quantum dot solar cells still remain locked away from the commercial market.

In Malaysia, a study has shown the use of DSSC modules can be a well-thought alternative to silicon PV panels when it comes to the construction and powering of greenhouses. The roof of a greenhouse does not always require to be fully transparent, but this reduces the possibility of producing shade-intolerant plants,due to the silicon solar panels' shade. DSSC was proven to be a more effective solution for this niche plant market, since the DSSC is semi-transparent material, allowing the production of electricity as well as providing more sunlight to the plants [29].

Another ground breaking and futuristic market for 3rd generation solar cell materials, is the wearable photovoltaic technology. Some studies were conducted in this field using dye-sensitized solar cells (DSSC) as a solution for its flexibility, low fabricating costs and also their relatively high efficiency under weak illumination, since everyday objects are not constantly under direct lighting. The major feature for selecting the DSSC is the flexibility and its bending ease, because in a real scenario of creating a new type of clothing as a solar power source, it's imperative to select a

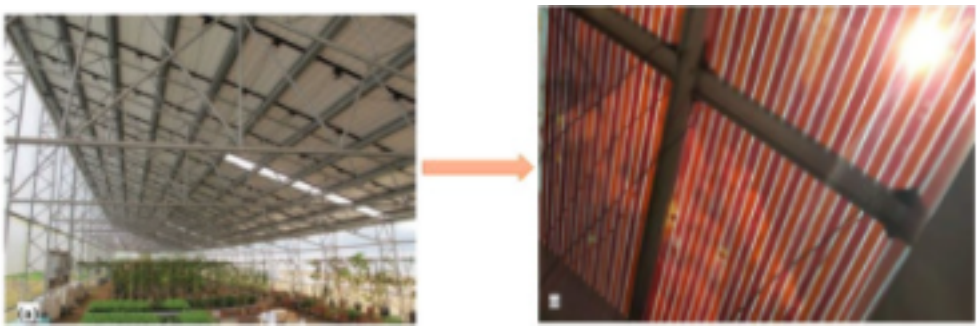

Figure 3.5: The evolution of greenhouse rooftops to DSSC panels. The semi-transparency of the DSSC (on the right) is the result of the type of dye at use, which acts also as a filter for the sunlight radiation. [29]

material that allows to behave like a textile and be robust enough to withstand deformations as the likes of rolling and folding. DSSCs have also sparked a few interests as well, not by its power conversion efficiency because it is not as high as other materials, but it caught the researchers' eye for its low cost production and (most importantly) small environmental impact.[21]

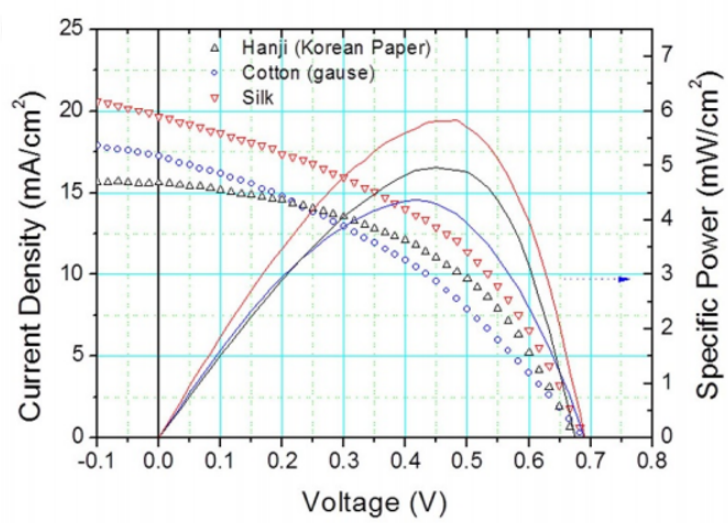

Figure 3.6: Current Density-Voltage characteristic and Power-Voltage curves for each type of analysed cloth fabric from Min Yun experiment. [53]

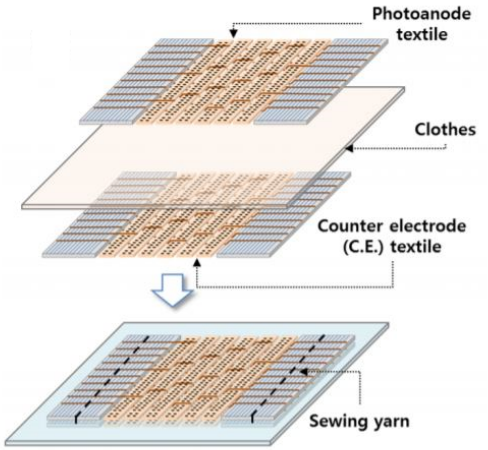

(a) Illustration of Min Yun's experimental textile-based dye-sensitized solar cell made after sewing textile electrodes to the fabric. [53]

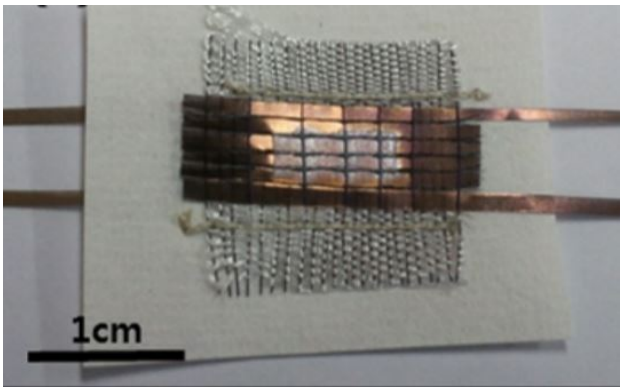

(b) Produced textile-based DSSC after sewing to Hanji paper [53]

Figure 3.7: Min Yun's experimental results for the creation of a textile-based DSSC.

In the studies conducted by Min Yun, it was developed a textile from different materials, with the main purpose of being sewn into different pieces of fabric, allowing the analysis of the solar cell in a more realistic environment. In the first experiment, it was taken into consideration the use of different types of fabrics and their performance under 1 Sun illumination. One of these fabrics was *Hanji*, a traditional korean paper, and the results can be enlightened by the obtained black current density curve in Figure 3.6. Registering an approximate short circuit current of $17\,mA\ cm^2$ and an open circuit voltage of about $0.7\,V$, resulting in a very low fill factor of 0.37 and an efficiency of roughly 5.3%, being its only limitation. Silk proved to have a higher impact than the others achieving an efficiency of almost 7%. Min and her co-workers concluded that there was still room for improvements in the materials used, since they had used conventional and commercially available materials, as well as improvements in the woven pattern, which was later tackled in the future experiments.[53][52]

The use of DSSCs as wearable solar cells unlocked a whole new concept of creating textile materials to enhance the power conversion efficiency, setting new challenges such as the adaptation of some materials used for the different components of DSSCs, like electrodes, electrolytes and so on.

3.2 Industrial Production

When it comes to the production of the cells at hand, there are a few differences. Due to the market size and lifetime, the silicon PV industry is much more advanced and ready than the other types of solar cells, such as the thin-films. Nonetheless, the other generations have some methods of their own, that are still picking up momentum to reach a much larger audience. The best example is the flexible thin-films because it can achieve a possible mass production level once operating in a traditional industrial manor, that will be further discussed in this section.[3]

Silicon-based cells, like it was seen before, can be produced in a more pure crystalline form (mono-Si) or through cheaper alternatives (poly-Si). Either way, both are turned into ingots that are later sliced to produce the silicon wafer that will be used to make PV panels [8].

(a) Slab of poly-Si after growth.

(b) The ingots of silicon must then be sliced into smaller blocks, which are later cut up into wafers through wire saws.

Figure 3.8: Industrial production of polycrystalline silicon [8].

One-step deposition is the most common method produce thin film solar cells. The substrates and layers are deposited through spin-coating, which technique is depicted in Figure 3.9. Then it is mixed the rest of the other compounds on the turntable and it's taken to another spin applying the same method. While the plate is spinning, the materials are always under the annealing temperature and this temperature has to set to a certain value for it to reach the best PCE (usually about 100^{o}C).[17][51]

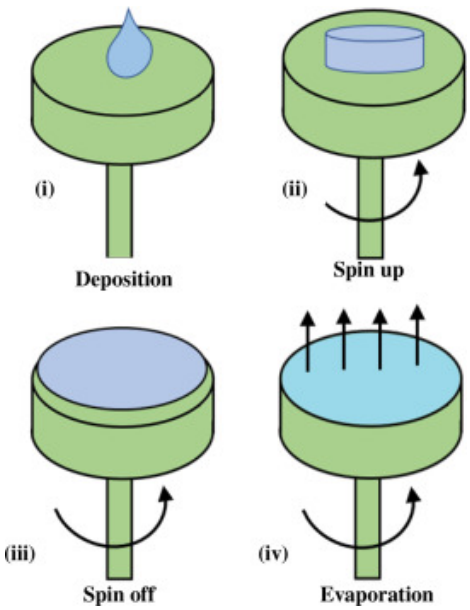

Figure 3.9: i) the material is deposited on the turntable ii) the turntable start accelerating applying centrifugal force, thining the layer iii) the turntable decelerates iv) throughout the process the plate will heat up and remove high volatile compounds and drying the rest of the substrate.[51]

At the moment, spin-coating is the most popular method for fabrication of 3rd generation thin films in lab-scale

devices, through deposition, such has DSSCs and PSCs. This method can hardly be replicated in an industrial format because this method wastes a lot of material that is ejected from the substrate once in rotation. Also, if the size of the substrate is too big, the high-speed spinning becomes more difficult.

When considering CIGS thin-films, spin-coating isn't necesserally the best procedure to develop CIGS absorber layers and cells.

One of the best techniques to produce CIGS modules is the **SAS** - sulfurization after selenization - produced by T.Kato, which consists of a method cadmium free. Firstly, it starts with selenization which is the crystal growth process, forming the $Cu(In, Ga)Se_2$ compound, determining the whole arrangement and structure of the crystal [22]. This can be done either the use of a toxic chemical, H_2Se to selenize the metals, or through rapid thermal processing (RTP), where Se is coated on top of the CuInGa compound, while sequentially under low and high temperatures.

The next step is sulfurization. A straight forward step consisting of the deposition of sulfur on the top of the CIGS layer, supressing any front interface recombination. This procedure grants about 22% of efficiency to the CIGS cell which is a very promising result.

Despite the high efficiency results for CIGS, these methods are still limited when adopting to a more industrialized scale, because they are very specific and very expensive.

Recently, the best way to reduce the pricing of thin film cells and maximize their throughput is by the implementation of a roll-to-roll (R2R) production. To reach such aspired goal, the fabrication method had to be switched to printing techniques, which were more compatible with R2R.

In a more traditional overview, R2R processing is a fabrication practice that has its roots in the manufacturing background, with the intention of embedding, coating, printing or laminating numerous applications onto a flexible rolled substrate material that is continuously passed on from one roller to another. As the materials pass on from roll to roll, different actions will take place between them, such as the ones mentioned above, in a chain of events that will lead to a final product. Essentially, this technique has vast variety of applications and sectors that require flexible material for completing a finished product.[40] Covering from textiles and paper, all the way to electronics and PCB boards, the roll-to-roll mechanism has proven to be a very well known technology in the industrial department and applying this very well-established mechanism to PSC fabrication can spark a great increase in its mass production, making the PSCs to reach a more competitive price in the market.

Currently, the R2R fabrication is starting to be more recognized as a possibility in the production of thin film solar cells in an industrial manor, promoting different types of techniques to manufacture these new panels, so to better visualize the fabrication procedure Figure 3.10 exhibits a pilot solution provided by a few scientists lead by Young Yun Kim of what it looks like to establish a R2R PSC manufacture. The target of this pilot-scale R2R machine, was to test the **gravure printing** technique they developed, which can deposit and pattern a desired layer at once through high precision, like a printer.[14] [23] [28]

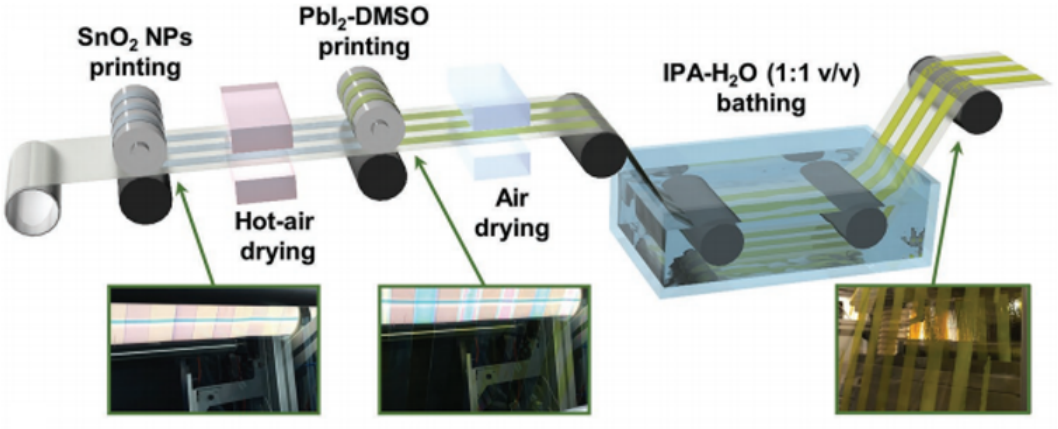

Figure 3.10: Illustration of the roll-to-roll system for PSC prodcution [23]

3.3 PV Waste, Recycling and Toxicity

Production of clean energy came as a solution to reduce the impact of fossil fuel as an energy source. Although its huge contribution to the reduction of the planet's carbon footprint, photovoltaic applications have their own lifecycle. Once it has reached its end, the PV module or device starts to be seen as electronic waste. Throughout their life time, panels decrease their efficiency and need to be replaced by new ones, after a few decades. Most of the PV waste ends up in landfills, and given the presence of numerous toxic materials, it can lead to a dangerous source of pollution, such as the pollution of ground waters. [14] Despite the environmental hazardous materials, some of modules contain valuable metals such as Silver, Copper and Gold which can be extracted for re-fabrication purposes, therefore bringing an extra value for recycling these metals and materials. [14]

Thus the need of recycling this type of waste is necessary and luckily this subject is already being taken into consideration by the European Commission, providing the Waste Electrical and Electronic Equipment (WEEE) Directive. [30]

Silicon waste is one of the main concerns when developing PV systems, because 94% of the solar cells produced use crystalline silicon, roughly translating into 400,000 tones of this material. The major problem at hand with the reuse of old silicon PV panels back into production, is the high purity of the silicon itself. To produce a Si module, about 40% of it is lost in the wafer slicing and multi-wire sawing which the designated term to refer to this waste is the Kerf loss. [27]

Despite the importance of recycling and reusing used up silicon from old panels or industrial silicon waste, the procedures for rehabilitation are very energy demanding and economically impractical. High purity silicon manufacturing is a very energy intensive process as well as applying recycling methods for the intensive production. [16]

Furthermore, methods for recovery of Kerf loss have also been under analysis. Changqiao Yang et. al has shown a procedure to recover high-purity Silicon from PV waste, through superconducting high gradient magnetic separation (HGMS) technology. The wasted material is converted into a silicon paste that is fed into an inlet that passes through a high gradient reactor (with a steel wool filter) surrounded by superconducting magnets, pushing to the filter all the metal compounds, allowing non-magnetic particles (silicon powders) to escape through an outlet, Figure 3.11 can show a better representation of the HGMS. [49]

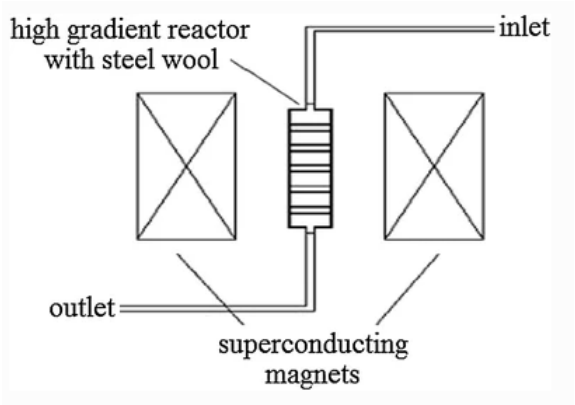

Figure 3.11: Schematic of the superconducting high gradient magnetic separation used by Changqiao Yang [49].

The superconductive HGMS proved to be an effective solution for silicon powder purification from kerf loss slurry waste, considering fine magnetic particles can be removed. In Figure3.12 it's clearly observable the SEM iamges of the before and after result of the HGMS process, increasing the percentage of silicon in a sample of slurry kerf loss, from 78.31% into 91.27%. [49]

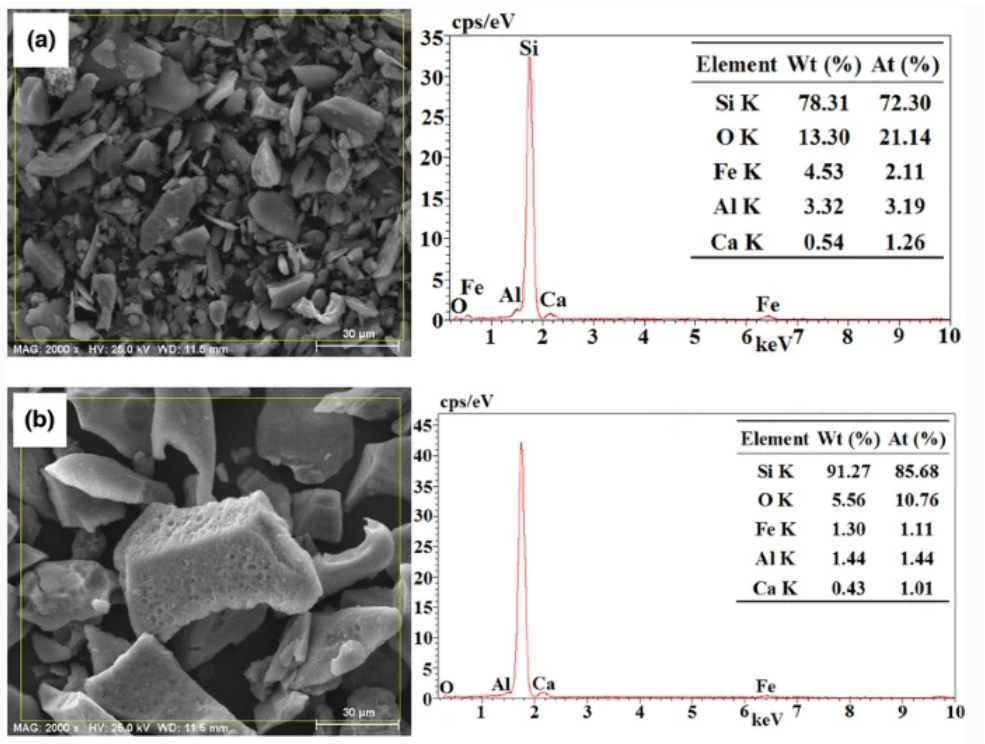

Figure 3.12: SEM images of raw material (inlet) and magnetic concentrate (outlet). a) Raw material b) magnetic concentrate [49]

Thin-films however are known to provide a low cost and flexible solution when compared with other previous cells, using only small material quantities. In spite of using very little quantities, most of the materials used are extremely toxic and environmental hazardous is disposed incorrectly, such as cadmium. CIGS for example can be produced without a cadmium buffer layer, but it will hurt its high efficiency. [31]

Ilke Celik et. al shows exactly the consumption of several resources such as electricity and materials. Table 3.1 better summarizes the whole recycling procedure for a $1m^2$ CIGS solar panel. [10]

Table 3.1: Recycling procedure for $1m^2$ of CIGS PV panel, featuring the amount of consumed materials for recycling as well as the energy consumption to recycle and unrecyclable materials. [10]

Process steps	**Material consumption**
Crushing	-
Acid Leaching	H2SO3 (750g); H2O2 (23g); surfacant (23g)
Skimming and filtration	NaOH (330g)
Precipitation and filtration	SO2 (75g)
pH adjustment	-
Indium extraction	D2EPHA (30g); Toluene (120g)
Stripping	HCl (750g)
Electrodeposition	-
pH adjustment	NaOH (105g)
Gallium extraction	D2EPHA (36g); Toluene (145g)
Stripping	NaOH (900g)
Electrodeposition	-

Disposable materials:	620g wiring plastic for incineration
	130g contaminated glass, disposed in landfill

Total energy consumption:	4.4 kWh

When it comes to the third generation of photovoltaic technology, the ecological effects are much more taken into consideration. This can be seen for example in the development of OSC, a solar cell fully functioning solar cell made exclusively with organic materials. Although PSC contain lead and inorganic materials (hence the name hybrid perovskite), some adjustments have been made for the substitution of lead for tin, a much less hazardous material than Pb, as well as the study of procedures to refurbish PSC through layer removal, while maintaining a good performance.

Another of these third-gen materials are the DSSCs. DSSCs can have a more eco-friendly design, since it behaves as a more electrochemical device, so the use of natural dyes and bio-based carbons is a very good sustainable alternative. Despite it's sustainable advantage, this type of DSSCs are difficult to recycle due to the utilization of nanostructures. Simpler nanostructures allow a higher recycling rate of success, but produce a lower outcome. However, there are emerging studies and projects being developed that allow the application of complex nanostructured materials that have a high recyclability.

Chapter 4: Simulation

Solar cells can be seen as an optoelectronic device, which means they can be seen from either an optical or an electrical point of view. To represent the model of a solar cell it was used a Finite Element Tool. This type of tool is used in diverse areas of physics and engineering, allowing the user to model a required object and subject it to a wide range of operational conditions and physical effects, all the way from fluid dynamics to quantum mechanics. Included in all this huge variety it is undoubtedly possible to perform a simulation in the optoelectronics field. This means, a device such as the solar cell can be recreated into a 2D or a 3D model to better study the behaviour of such device.

Throughout this report, an electrical approach was selected to be the main target of the model. However, this does not imply that the model lacks any optical features, since optical properties for several materials were taken into consideration for the calculation of the results.

4.1 PIN structure model

As it was seen in the previous chapters, a solar cell at its core is seen as a p-n junction, that can convert light into a current. Incident photons with energy larger than the band gap can be absorbed by engaging with an electron from the valence band and exciting it into the conduction band, leaving a hole behind in this band. Despite this conjecture for solar cells being seen as mainly p-n junctions, these devices can also adopt another type of displacement, the **PIN** structure.

A PIN or NIP structure (p-i-n or n-i-p) consists of 3 layers of semiconductors, rather than the 2 layers in p-n junctions, the p-type layer and the n-type layer. The PIN structure adds another layer, specifically an **intrinsic layer**, between the two extrinsic semiconductors.

By adding this intrinsic layer (i-layer), it is possible to reduce the surface recombination, which has an influential role on the generated current of a solar cell, especially on small area ones [19]. The i-layer also provides a wider depletion region, increasing the minority carrier diffusion length as well as strengthening the charge carrier lifetime (which reduces recombination).

PIN structures are widely used in certain types of solar cells. GaAs solar cells have incorporated PIN structures into their own design. Yao Wu et al. developed a PIN AlGaAs/GaAs heterojunction (Figure 4.1), where the AlGaAs, a material with very low absorption coefficient, is used for the p-layer. This reduces the generation of photocarriers in the p-region, but once it reaches the i-layer, more photocarriers are concentrated, supressing the recombination loss caused by high doping concentration, as well as deflecting minority carriers away from the surfaces/contacts to decrease minority carrier recombination. [48]

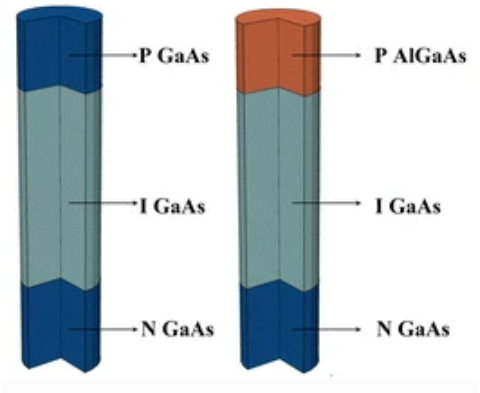

Figure 4.1: Schematic drawing of the GaAs nano wire solar cell (left) and its heterojunction counterpart the AlGaAs/GaAs solar cell (right), both used by Yao Wu et al.[48]

The used model and all the simulations for this study was designed and accomplished using the COMSOL Multiphysics software, a Finite Element Tool that specializes in the computation of complex physical models from all the different fields of engineering.

This same model was based on a 2D sample model for a GaAs PIN photodiode from the application library of COMSOL. A photodiode and a solar cell are both electronic devices produced from the same structure, but operating at different regions of the I(V) characteristic. The photodiode operates in reverse bias while the solar cell does not require any bias, therefore some adjustments needed to be made before starting any simulation.

To better understand the model at hand, Figure 4.2 facilitates the comprehension. Breaking down into a more detailed approach of the PIN layers of the generated 2D model. As it was demonstrated before, the PIN module is composed by 3 layers: p-layer, i-layer and n-layer. For this 2D model approach, the same layers were taken into consideration, however as it can be seen in the schematic.

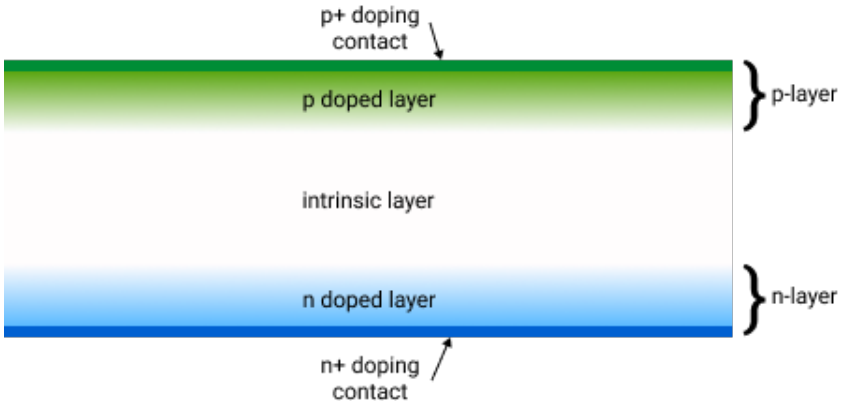

Figure 4.2: Illustration of the used solar cell PIN model.

First of all, it is important to clarify that the intrinsic layer is not defined by the user, but generated from the definition of the carrier densities of each p and n layers.

The p-layer and the n-layer are both composed by a heavily doped contact at the top (p+) and bottom (n+) of the cell respectively. In addition, there is also a larger p and n doped areas that contain less dopant (about 100 times less).

The role of this second layer is to facilitate the diffusion of the carriers throughout the solar cell, in order to generate the intrinsic layer in between. Figure 4.3 shows the dopant concentration throughout the entire cell, hence the null charge zone represents the depth of the generated intrinsic layer.

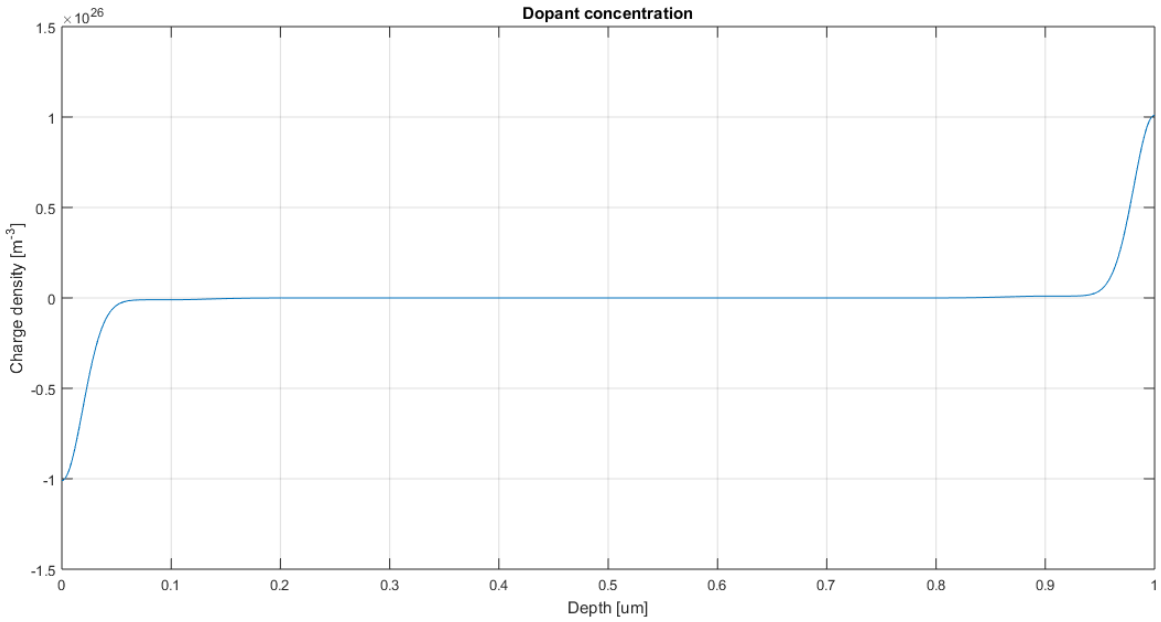

Figure 4.3: Dopant Concentration.

After successfully creating the 2D solar cell model, the simulations were ready to start. Since the goal of the simulations were to examine some electrical and optical properties for different generational PV materials, the **responsivity** and the **current-power relationship** were the chosen properties to examine that could be successfully achieved.

GaAs can be considered as 2nd generation material, although for some researchers it is still considered as a 1st generation material.

The main targeted materials in this section is the Silicon, GaAs and CIGS. GaAs can be considered as 2nd generation material, although for some researchers it is still considered as a 1st generation material, but the important information to retain is that GaAs is an heterojunction, and its role in this study is to add another comparison with CIGS, since it is also an heterojunction.

In addition, CIGS is also a material that must be treated somewhat differently, for two reasons.

- The CIGS solar cell is comprised of many other layers. And as it was seen before the absorber layer, CIGS, acts as the p-type material of intire cell;
- CIGS has a few properties, such as the band gap and the electron affinity and , that depend on the concentration of gallium.

In this particular case, for the n-layer section of the CIGS PIN model, the donor density used will be equal to the doping of the CdS buffer layer, simulating the interface between CIGS and the buffer.

The gallium dependent values for CIGS offer the possibility to conduct a deeper study of the responsivity and current-power relationship for different concentrations of CIGS.

CIGS is nominated by $CuIn_{(1-x)}Ga_xSe_2$ with x being defined by equation 4.1.

$$x = \frac{\text{Ga}}{\text{Ga} + \text{In}} \tag{4.1}$$

Previous studies of the CIGS material, from Isabela et. al and P.D. Paulson have used specific values for the concentration of Gallium to compute their results [41] [7]. The results can be observed in Table 4.1.

Table 4.1: Band gap and electron affinity values for each percentage of gallium in CIGS, given by Isabella et. al study [7]. To $x = 0$ the CIGS solar cell has no percentage of gallium, thus holds the name CIS, while the same can be said for $x = 100$, the cell has no Indium, therefore CGS.

	x	Band gap (eV)	Electron Affinity (eV)
CIS	0	1.023	4.57
CIGS-31	0.31	1.208	4.25
CIGS-45	0.45	1.351	4.1
CIGS-66	0.66	1.457	3.93
CGS	1	1.771	3.87

Before jumping into the simulation, it is important to establish the properties of each material that will be used in the simulations, as well as the standard values of the model (Table 4.2).

Table 4.2: Values of the required parameters to simulate the solar cell model. Only the electron affininty and the band gap are gallium dependent variables, the others have no dependency.

		Silicon	**GaAs**	**CIGS(100 - 0 Ga)**
Relative permittivity	ε_r	11.68	12.9	13.6
Band Gap (eV)	E_g	1.12	1.424	1.771 - 1.023
Electron affinity (eV)	χ	4.05	4.07	3.87 - 4.57
Effective density of states Valence band (cm^{-3})	N_v	$(\text{T}/300)^{3/2} * 1.04E19$	$(\text{T}/300)^{3/2} * 1.83E15$	$(\text{T}/300)^{3/2} * 1.5E19$
Effective density of states Conduction band (cm^{-3})	N_c	$(\text{T}/300)^{3/2} * 2.8E20$	$(\text{T}/300)^{3/2} * 8.63E13$	$(\text{T}/300)^{3/2} * 6.8E17$
Electron mobility ($cm^2/(V \cdot s)$)	μ_n	1450	8500	1
Hole mobility ($cm^2/(V \cdot s)$)	μ_p	500	400	15
Carrier lifetime (s)	τ	2E-9	2E-9	2E-9

Width (μm)	**l**	5
Depth (μm)	**d**	1
Incident Power (W)	P_{in}	100

4.2 Responsivity

There is a different type of absorption spectrum for each material. For solar cells it is important to study how does the wavelength affect the behaviour of the cell, especially when it comes to the generation of electric current. The

responsivity grants the relation between the generated current from the solar cell with the emitted radiation power, or in a more practical term, it relates how much current does the device generate in 1 Watt of incident power. This metric is very useful to evaluate the performance of solar cells under a specific light spectrum.

In this study, the different solar cell materials will be tested with the PIN model, with the primary goal of validating the model, by checking how similar do the responsivity curves match the already known curves of the referred materials. Secondly, registering the I(λ) characteristic will also take great part in the justification of future values on the next analysis. To compare the obtained results it was used the responsivity from Figure 4.6, which represents a standard value of this metric for different photovoltaic materials. It's important to notice that converting the units does not change the shape of the curve.

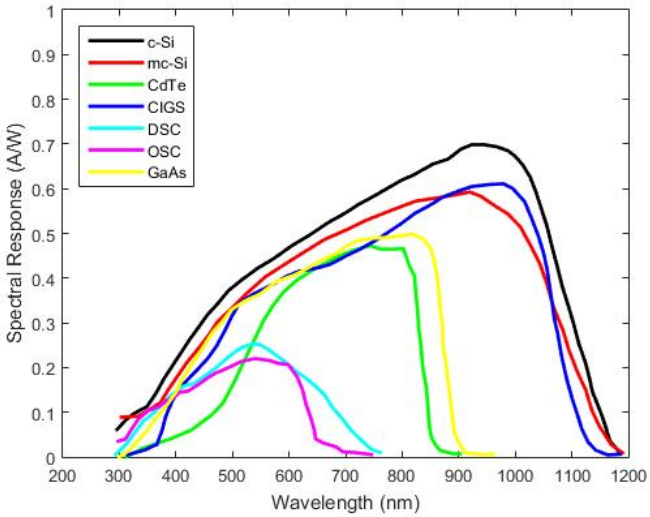

Figure 4.4: Responsivity for different solar cell materials, including CIGS, GaAs and Silicon solar cells. [6]

4.2.1 Silicon

Firstly the silicon solar cell was the first material to be tested. The results for this material are found in Figure 4.5. Silicon has an absorption band of about $740nm$, starting to absorb radiation at the $370nm$, which means for UV radiation, Si solar cells cannot work properly.

Then as the wavelength increases, it is possible to check a steadily rise in the materials responsivity, generating higher currents throughout the whole visible spectrum, but for Infra-red radiation, silicon has a huge spike, achieving a maximum of $0.778\mu A/W$ at $1030nm$.

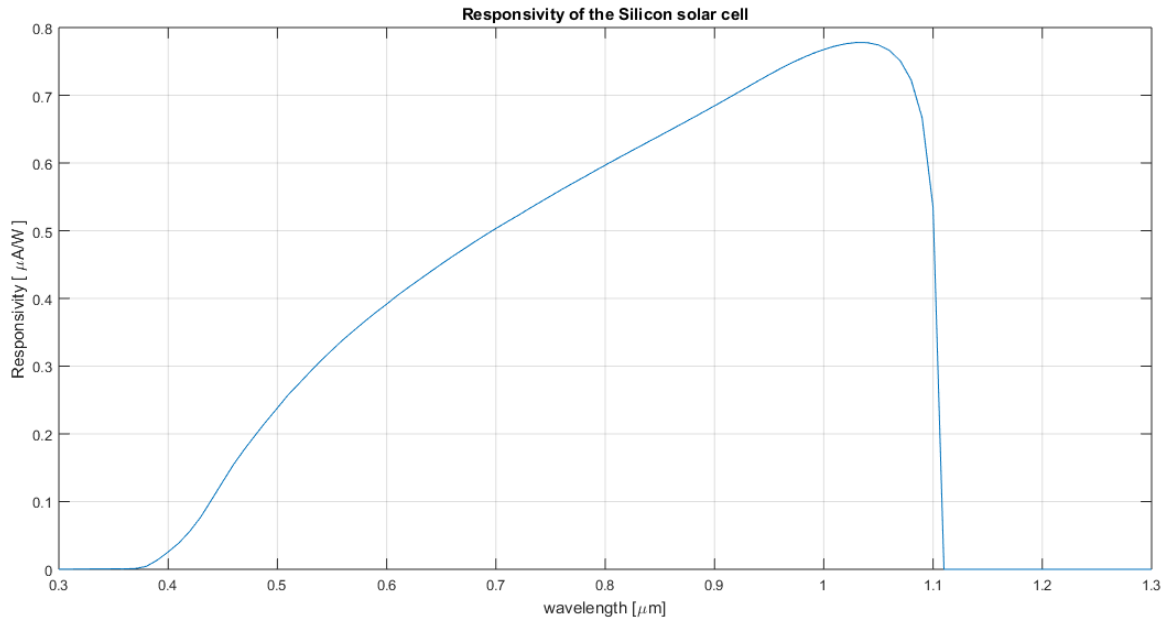

Figure 4.5: Responsivity of silicon

4.2.2 Gallium Arsenide

Secondly, there is the Gallium arsenide solar cell. This cell has a much shorter absortion band ($646nm$), since the band decreases drastically after the $240nm$. The maximum peak of responsivity happens for radiations which fall a bit short after entering the IR region. So the GaAs has a very good responsivity and absorption for radiations within the visible spectrum.

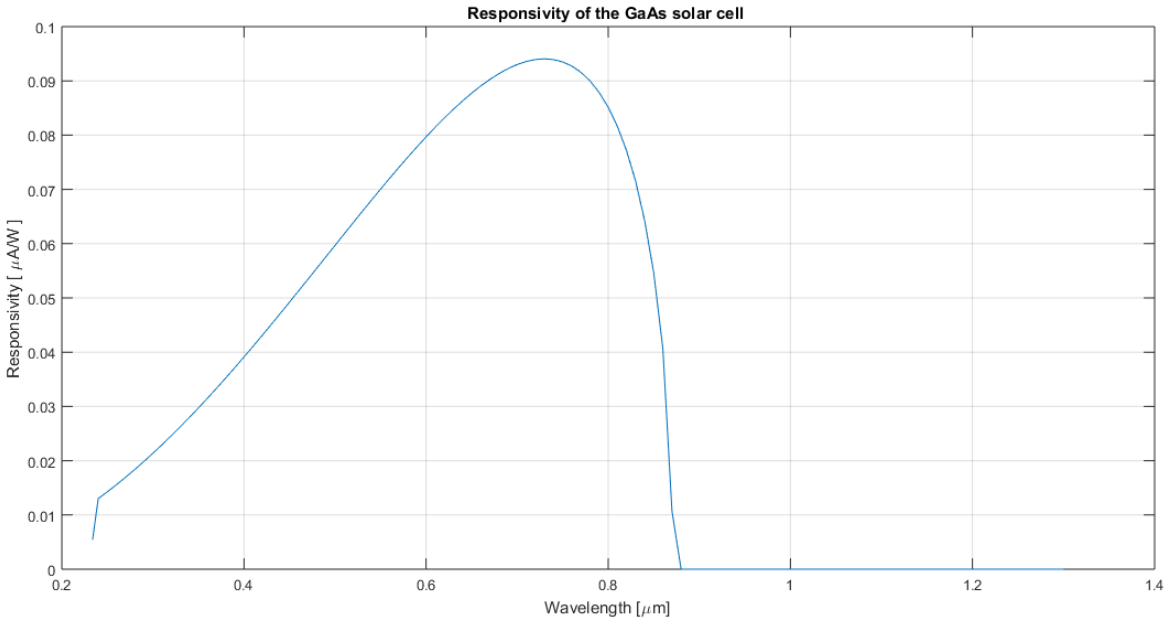

Figure 4.6: Responsivity of GaAs

4.2.3 CIGS

For the CIGS responsivity, the concentration of Gallium was taken into consideration, due to the influental role it was when determining certain material properties.

After running the simulation for different concentrations of gallium, it is clearly possible to visualize a decrease of the wavelength for maximum responsivity, as the concentration of gallium increases. This reaction is logical since the increase of gallium within the CIGS cell increases its band gap, thus narrowing its absorption range. The responsivity also decreases when the gallium concentration is increased.

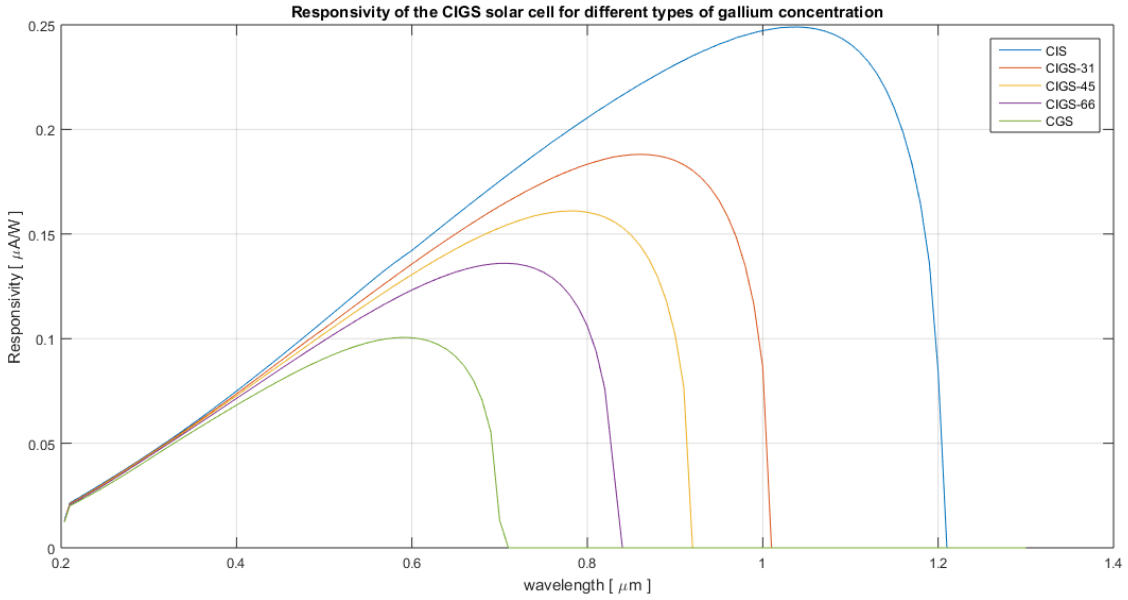

Figure 4.7: Responsivity of CIGS

4.2.4 Overview

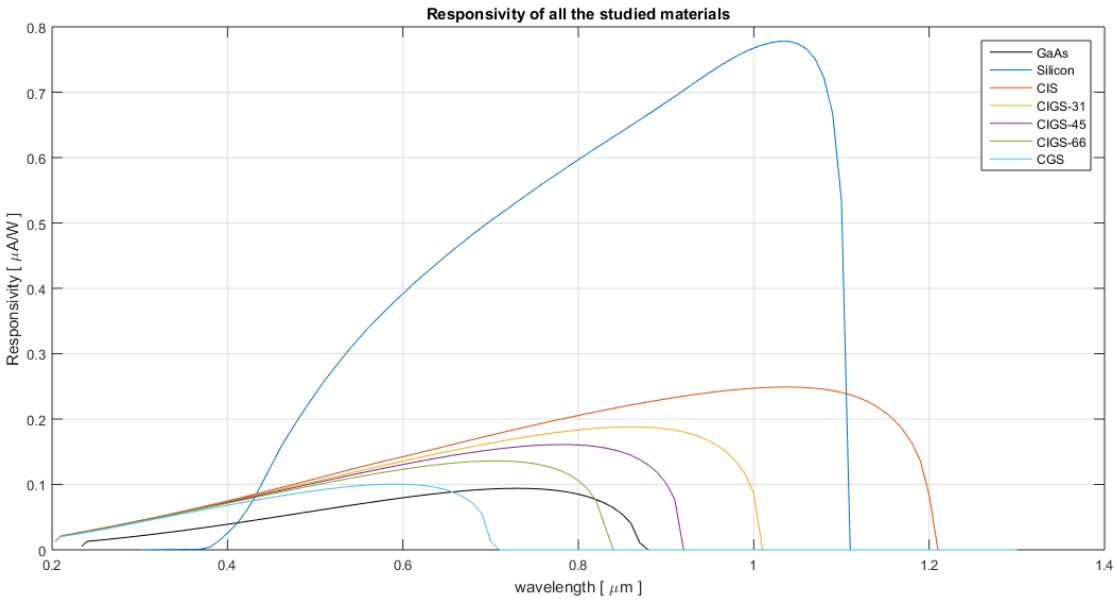

Figure 4.8: Responsivity of CIGS

After analysing each material individually, it is necessary to compare all curves to extract more conclusions of the model and of the materials.

Starting from the comparison of the simulated results with the theoretical curves from the literature, at first sight the responsivity values are much smaller for the simulated results than the others, since one is given in A/W and the other in $\mu A/W$.

A potential reason for that deviation could be given by the area of the simulated solar cells. This area is relatively small when comparing to other solar cells, since the original area was extracted from the photodiode model, which are known to contain very small areas, hence creating these possible discrepancies.

The CIGS solar cell presents itself on the simulation with very low responsivity, when on the theoretical data, the results are relatively close to the silicon solar cell. Since a CIGS cell is composed of more other 3 layers (minimum), each of them with their own band gap and doping density, it could explain why the generated current per incident power is so low, as the CIGS absorber layer requires the presence of the other layers in order to unlock its full potential. However, the theoretical results do not reveal the concentration of Ga, but this previous reason can also play a crucial role in widening the absorption band, since the theoretical CIGS has almost the same absorption range as the simulated CIS.

Nonetheless, the results for the 1st generation solar cells have proven to be more close to theoretical case, than the 2nd generation cell. This could also mean a possible relationship between the adoption of a PIN structure vs a normal p-n juntion structure, despite the theoretical results not having any information of the type of structure at use, but in any case it is possible to conclude that the approximations made are very similar to the theoretical curves.

4.3 Current-Power relation

The next simulation to be executed is the Current-Power relation. The goal of this simulation is to check the linearity between the generated current of the solar cell, I_L, and the incident radiation power, P_{in}.

It is estimated that the for 1st generation materials, the current increases linearly with power. However, the same statement may not be entirely true, since other 2nd generation materials are composed of much more complex heterojunctions (4 junctions in case of CIGS absorber layer).

To better represent the correlation of current and power obtained from the output data of the model, it was used the *polyfit* function from *MATLAB* to find the equation that best fit the data. The polyfit function is a MATLAB function which returns the coefficients for a polynomial $P(x)$ of degree n that best fits its input data, described in 4.2.

$$P(x) = p_n x^n + p_{n-1} x^{n-1} + p_{n-2} x^{n-2} + ... + p_0 \tag{4.2}$$

The model allows the possibility to specify the type of desired radiation, according to its wavelength. So, to determine the I(P) curve, the wavelength of the material was taken into consideration, granting a more thorough study of the cell for specific regions of the light spectrum, yielding much more complete results of the I(P) curve. The chosen wavelengths were selected to represent each region of the visible spectrum, as well as the ultra-violet region (UV) and the infra-red region (IR). The specified wavelengths are shown in Table 4.3.

Table 4.3: Selected wavelengths to study the I(P) curves

Spectrum region	UV	Blue	Green	Orange	IR
Wavelength [nm]	300	420	550	690	800-1100

For the IR region, due to the different absorption limits of the materials, the standard value that was $900nm$, can either surpass the absorption range of the material, or isn't close enough to the maximum absorption point.

4.3.1 Silicon

As the light is shed upon the silicon surface, it is possible to register the current change, as the power was increased, obtaining the results in Figure 4.9. As it can be seen, for all the studied wavelengths the generated current from the solar cell has a linear relation with the incident light's power. Starting from the UV wavelength, the absorption of the silicon cell is very close to zero, since the responsivity for silicon solar cells at the UV mark is practically null. As the wavelengths are increased, the slope of each function increases as well, since the responsivity of silicon reaches its peak at $1000nm$, which corresponds to the IR region. For each wavelength, the curve that best fitted the data points was plotted, allowing the possibility to extract an equation that could relate the current with power, and for the silicon cell the best fit was a first degree polynomial equation, hence extracting the following values in Table 4.4.

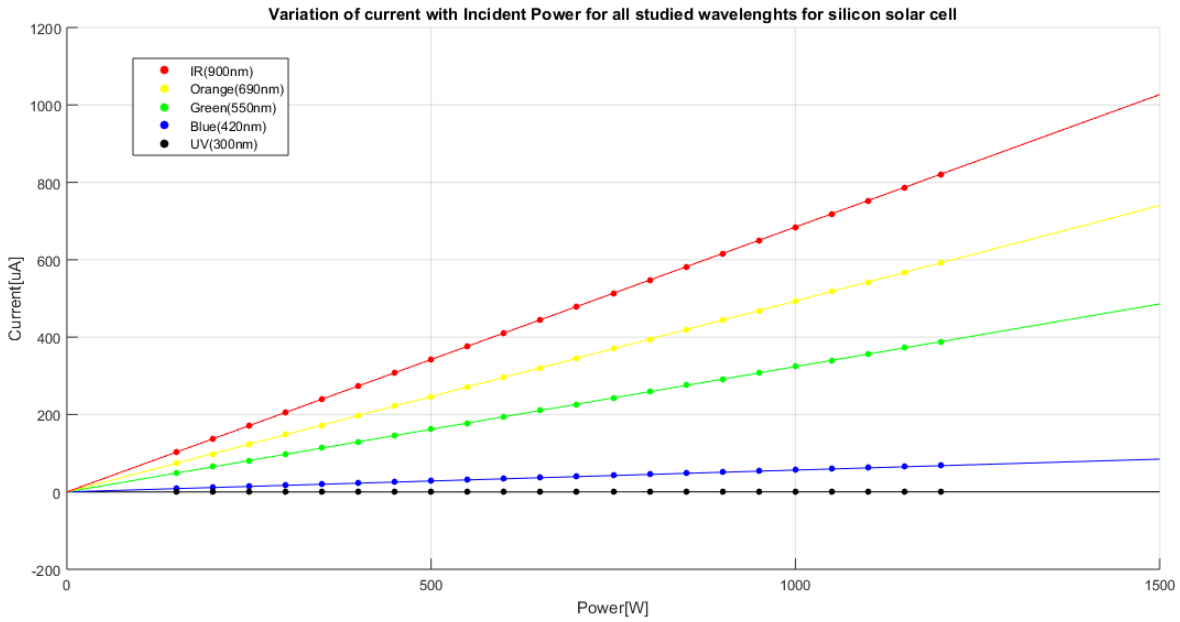

Figure 4.9: I(P) curve for Silicon solar cell.

Table 4.4: Extracted coefficients from the polyfit function of the Silicon solar cell I(P) data points

Wavelength	UV (300nm)	Blue (420nm)	Green (550nm)	Orange (690nm)	IR (900nm)
p_1	1.04E-4	0.057	0.324	0.493	0.685
p_0	5.87E-7	-3.09E-5	-0.001	-0.003	-0.006

4.3.2 Gallium Arsenide

Secondly, the Gallium Arsenide solar cell was submitted into the simulation. According to the responsivity of the GaAs material, it would be expected for the I(P) curve to have much better performance for the UV radiation over the Silicon material, since the conversion of UV radiation to current for the GaAs is larger than silicon. However, the maximum current is significantly lower than the silicon cell, and all of the slopes are much smaller than the ones obtained before, as it can be observed in the following Table 4.5, where p_1 represents the slope of each function. Once again the best fit the solar cell was a 1st order polynomial equation.

The results can be seen in Figure 4.10 and at a first glance it is possible to verify once again a linear relationship between the obtained data points, proving the linear relation between the incident power with the generated current from the GaAs solar cell, as well as the previous expectation of higher absorption in the UV region, leading to a higher current value in the I(P) function, unlike the silicon material. It is also possible to point out that the responsivity of GaAs for IR radiation is very low, which is a statement that can be easily backed by the IR simulation, since the I(P) line is just a bit higher than the blue radiation.

Table 4.5: Extracted coefficients from the polyfit function of the GaAs solar cell I(P) data points

Wavelength	UV (300nm)	Blue (420nm)	Green (550nm)	Orange (690nm)	IR (850nm)
p_1	0.025	0.0438	0.0692	0.0885	0.0478
p_0	-4.27E-6	-1.44E-5	-2.57E-5	2.46E-5	-6.73E-4

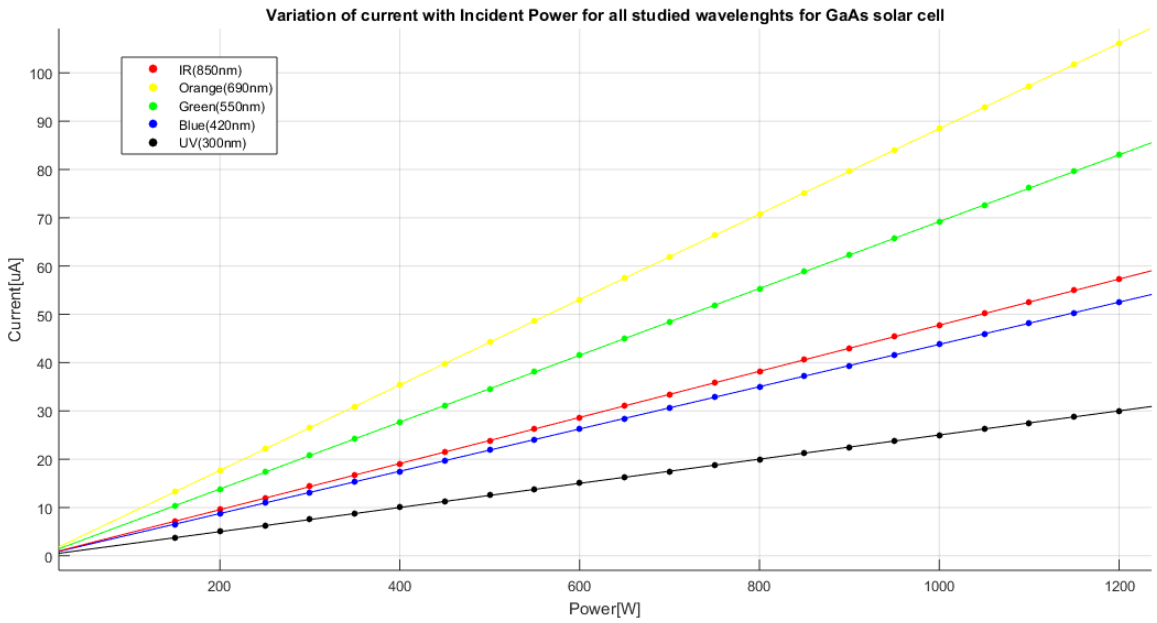

Figure 4.10: I(P) curve for GaAs solar cell.

4.3.3 CIGS

For the CIGS solar cell once more the gallium concentration was taken into consideration, owing to the effect it has on the responsivity of this material. Being this a more complex material, there should be some difference in the relationship between the irradiated power and the generated current as it was seen in the two previous materials. With this prospect, to ensure a correct reading of the I(P) function, the polyfit function was set accordingly to the equation that more closely defined the obtained data. While on the previous materials, a 1st order polynomial equation was what fitted best the output data, for CIGS, however, a 3rd order polynomial equation was the best fit.

The coefficients for each curve was also extracted for every type of CIGS as it can be seen in Table 4.6, Table 4.9, Table 4.8, Table 4.9 and Table 4.10. As it can be seen, the equation that better fit the results is a third order polynomial function, hence proving the non-linearity of the CIGS material.

CGS

As it was seen before, CGS holds the smallest responsivity window, since it stops absorbing radiation at $710nm$.

So, for the smallest wavelengths, around the UV mark, the CGS material presented to have a linear increase in current with the increase of power. On the other hand, once the wavelength starts increasing, the I(P) function starts to drift away from its linear shape, assuming a slightly curved shape. This small curved shape starts getting a bit more

noticeable as the wavelength increases. Along with the curving, the slope begins to increase as well, which is a natural response of the material's responsivity.

Nevertheless, once the wavelength for maximum peak of current is surpassed (590nm), the produced current is decreased. This is why the green radiation can produce higher output currents, Figure 4.11.

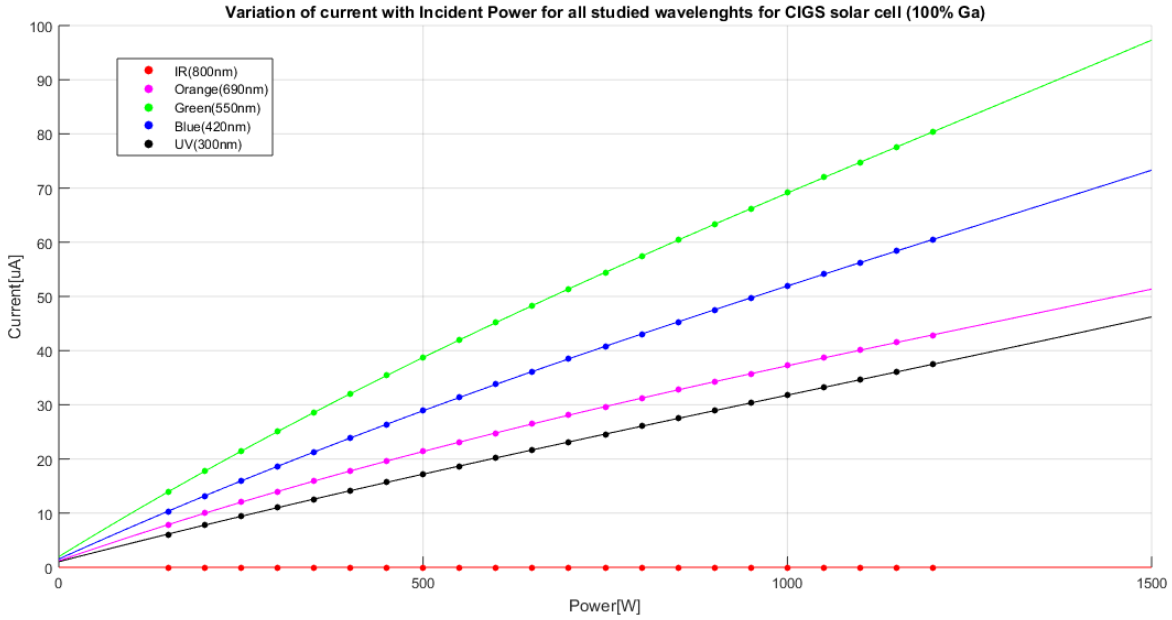

Figure 4.11: I(P) curve for the CGS solar cell.

Table 4.6: Coefficients of the 3rd order polynomial expression that best fitted CGS, for the different wavelegths.

Wavelength	UV (300nm)	Blue (420nm)	Green (550nm)	Orange (690nm)	IR (900nm)
p_3	1.906E-9	3.598E-9	5.69E-9	-3.588E-9	-
p_2	-5.998E-6	-1.409E-5	-2.132E-5	-1.411E-5	-
p_1	0.0348	0.0609	0.083	0.047	-
p_0	1.045	1.529	1.973	1.20	-

CIGS-66

For the CIGS-66 solar cell the simulated orange light achieves the highest generated current of the remaining wavelengths under study, more specifically $108.5\mu A$ for a $1200W$ incident power.

The lowest values of current is now held by the UV radiation, since the CIGS-66 reaches the maximum wavelength limit of absorption at $840nm$. However, to obtain a better reading of the CIGS-66 cell, it was used the $800nm$ value, avoiding also another null value, just to better showcase the IR region. Moreover, the UV region, once again, has a roughly linear relation between power and current.

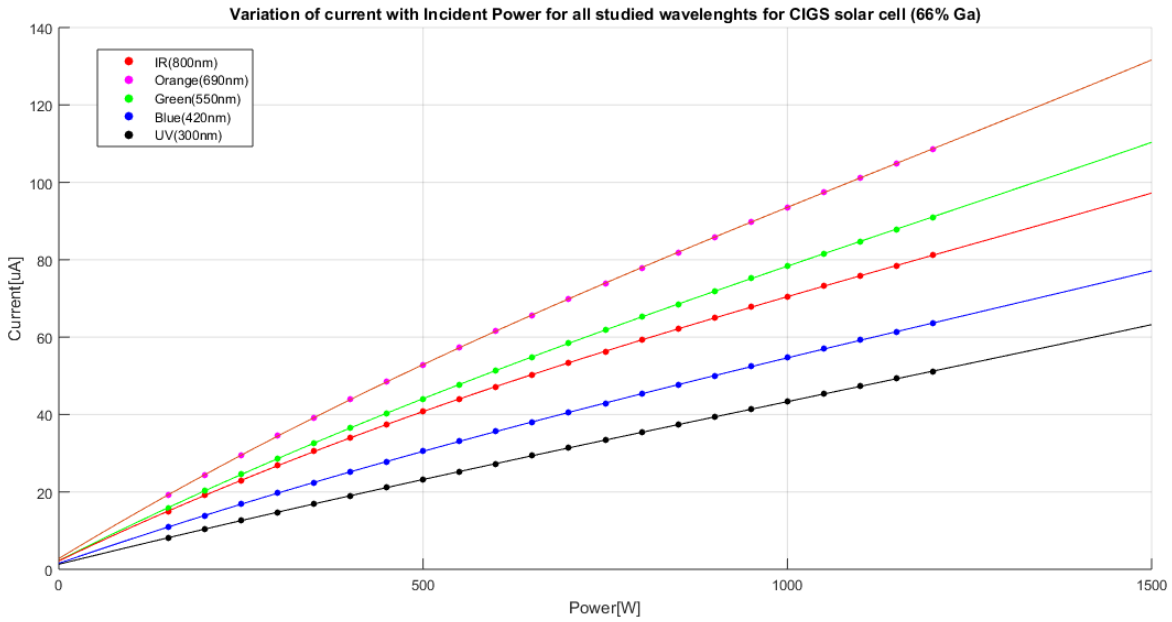

Figure 4.12: I(P) curve for the CIGS-66 solar cell.

Table 4.7: Coefficients of the 3rd order polynomial expression that best fitted CIGS-66, for the different wavelegths.

Wavelength	UV (300nm)	Blue (420nm)	Green (550nm)	Orange (690nm)	IR (800nm)
p_3	2.063E-9	4.094E-9	7.16E-9	9.251E-9	8.038E-9
p_2	-6.639E-6	-1.569E-5	-2.595E-5	-3.283E-5	-2.991E-5
p_1	0.047	0.065	0.095	0.1143	0.090
p_0	1.311	1.56	2.259	2.790	2.177

CIGS-45

CIGS-45 is the middle ground of the concentration of Ga within the PV cell. Much of the previous analysis can be spotted too, even with an increase of the absorption wavelength limit to $940nm$.

However, there is a much more intense curved shape for the IR radiation, then it was on the preceding results for IR. Nonetheless, the orange radiation continues to produce the highest current, but the highest peak in current is generated at the limit of the red/IR radiation, around the $780nm$ mark.

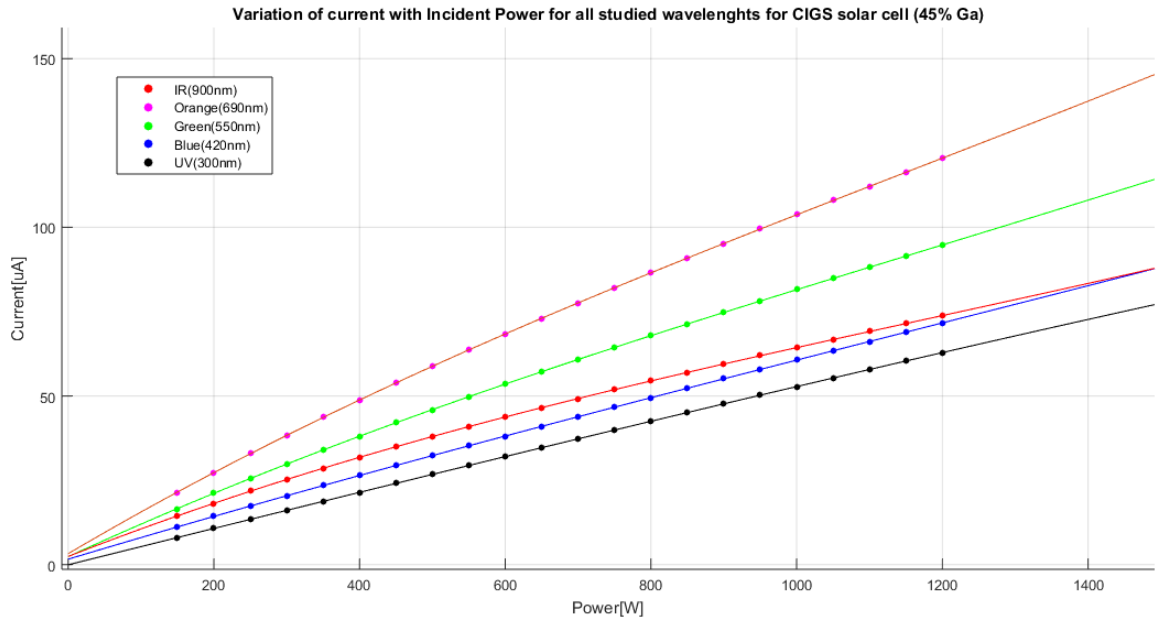

Figure 4.13: I(P) curve for the CIGS-45 solar cell.

Table 4.8: Coefficients of the 3rd order polynomial expression that best fitted CIGS-45, for the different wavelegths.

Wavelength	UV (300nm)	Blue (420nm)	Green (550nm)	Orange (690nm)	IR (900nm)
p_3	-7.805E-10	2.44E-9	7.728E-9	-1.077E-8	9.008E-9
p_2	-3.24E-7	-8.153E-6	-2.766E-5	-3.744E-5	-3.187E-5
p_1	0.0539	0.0649	0.0991	0.127	0.085
p_0	-0.0253	1.632	2.382	3.268	2.433

CIGS-31

Achieving a percentage of 31% of gallium within the solar cell, it is possible to verify that the IR radiation has surpassed the orange radiation when it comes to the generated current, achieving a maximum of 143.7μm. Nonetheless, no changes were found on the curvature of the I(P) function for each specific wavelength from the previous Figure.

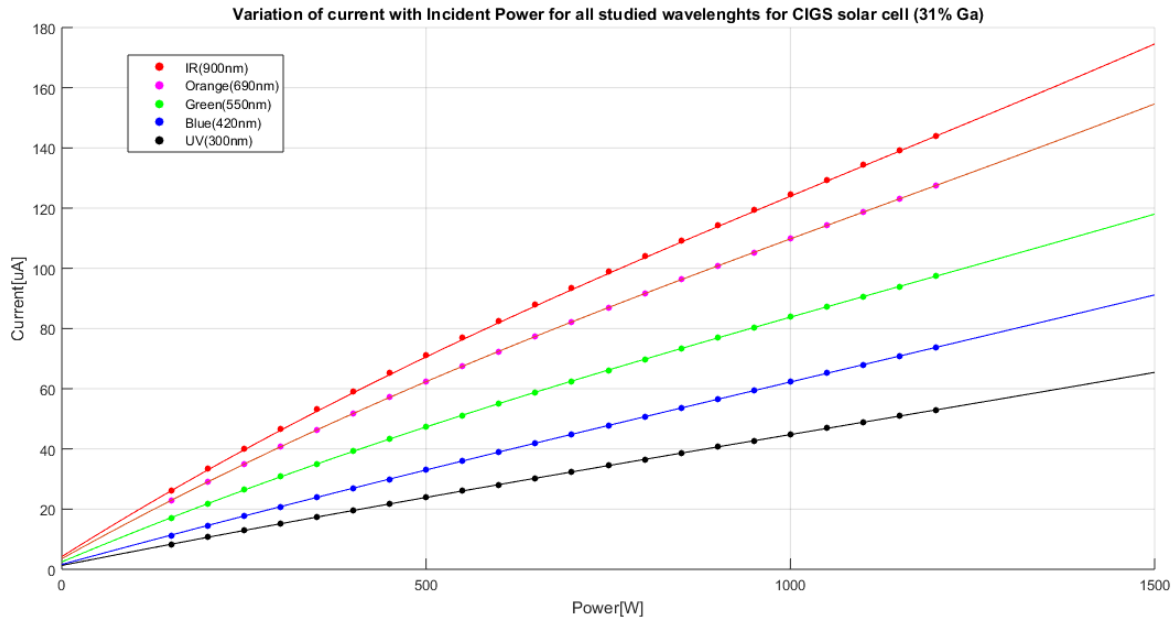

Figure 4.14: I(P) curve for the CIGS-31 solar cell.

Table 4.9: Coefficients of the 3rd order polynomial expression that best fitted CIGS-31, for the different wavelengths.

Wavelength	UV (300nm)	Blue (420nm)	Green (550nm)	Orange (690nm)	IR (900nm)
p_3	1.997E-9	2.456E-9	8.13E-9	1.169E-8	1.363E-8
p_2	-6.446E-6	-7.988E-6	-2.888E-5	-4.023E-5	-4.770E-5
p_1	0.048	0.066	0.102	0.135	0.154
p_0	1.284	1.622	2.468	3.557	4.245

CIS

With the CIS solar cell, the responsivity range reaches its maximum, thus the maximum current peak surpassed the maximum wavelength at study, so it was required to increase the study range for the IR region, so the $1100nm$ mark was added. This increase in the IR region, could prove that as the wavelength rises the non-linearity of CIGS increases further, since it is possible to get almost the same maximum current for both of $900nm$ and $1100nm$ wavelengths.

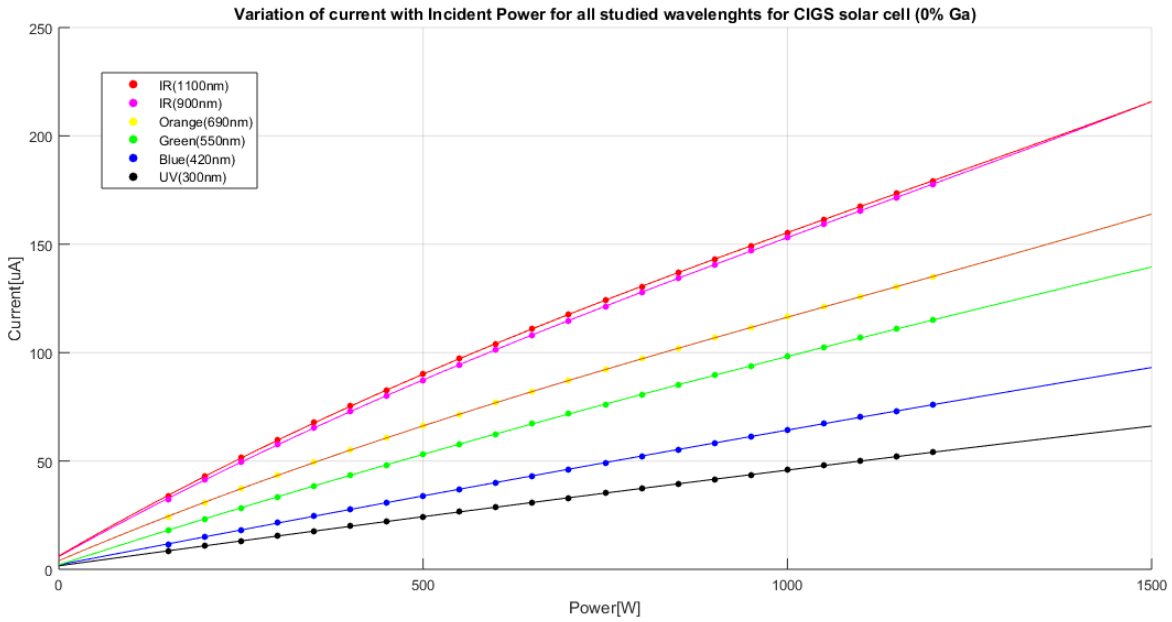

Figure 4.15: I(P) curve for the CIS solar cell.

Table 4.10: Coefficients of the 3rd order polynomial expression that best fitted CIS, for the different wavelengths.

Wavelength	UV (300nm)	Blue (420nm)	Green (550nm)	Orange (690nm)	IR (900nm)	IR (1100nm)
p_3	1.943E-9	2.414E-9	2.7E-9	1.270E-8	1.722E-8	1.838E-8
p_2	-6.279E-6	-7.846E-6	-1.571E-5	-4.32E-5	-5.749E-5	-6.475E-5
p_1	0.049	0.068	0.109	0.143	0.1875	0.196
p_0	1.255	1.593	2.042	3.987	5.869	6.173

On a general conclusion, after observing every I(P) function of the solar cell, it is safe to assume a possible relationship of the non-linearity to the increase of wavelength, since most of the non-linear results occur above the green radiation. This non-linearity can also be spotted in a more early stage, more specifically in the blue radiation for CGS, because the absorption range is very small.

A plausible explanation to this occurrence may have to do with some of the material properties of CIGS. Taking into consideration equation 4.3, power and the generated photocurrent can be related by

$$I_L \propto q \cdot P_{in}(L_n + L_p) \tag{4.3}$$

Given that q is the electron's charge, and both L_n and L_p are the electron and hole diffusion lengths respectively. However, the L_n and L_p can be given as an equation of the diffusivity, $D_{n,p}$, and the carrier lifetime $\tau_{n,p}$.

$$L_n = \sqrt{D_n \cdot \tau_n} \tag{4.4}$$

$$L_p = \sqrt{D_p \cdot \tau_p} \tag{4.5}$$

The carrier lifetime, τ, is the average time which a carrier can spend in an excited state after electron-hole generation before it recombines. This parameter depends a lot on the structure of the solar cell and the type of material.

For this reason in particular, different carrier lifetimes will be obtained for different types of materials (band gaps), hence different diffusion lengths will be obtained, leading to different current values that vary non-linearly.

Chapter 5: Experiment

This experiment has the goal to compare the electrical behaviour of different solar panels made from different materials, each representing a different technological generation of PV panels.

For this study, the efficiencies, fill factors and characteristic curves are the electrical properties of the PV panels that were evaluated. It was planned to test one type of solar cell material that represented each of the three generations of PV technology. **Crystalline silicon** (c-Si) was chosen to represent the 1st generation, **CIGS** the 2nd generation and **DSSC** the 3rd generation. The studies conducted to the crystalline silicon and the CIGS solar cell materials provided the required information to produce the necessary results.

However, the results obtained from the DSSC study were mainly inconclusive, since the DSSC cell had no contacts to connect the necessary equipment and measure the output voltage of the cell. Due to the small area of the DSSC ($2.04cm^2$) it was also expected to produce a very small output voltage and current, uncertain that the multimeter would be able to measure these signals, since it could have fallen off the range of the device.

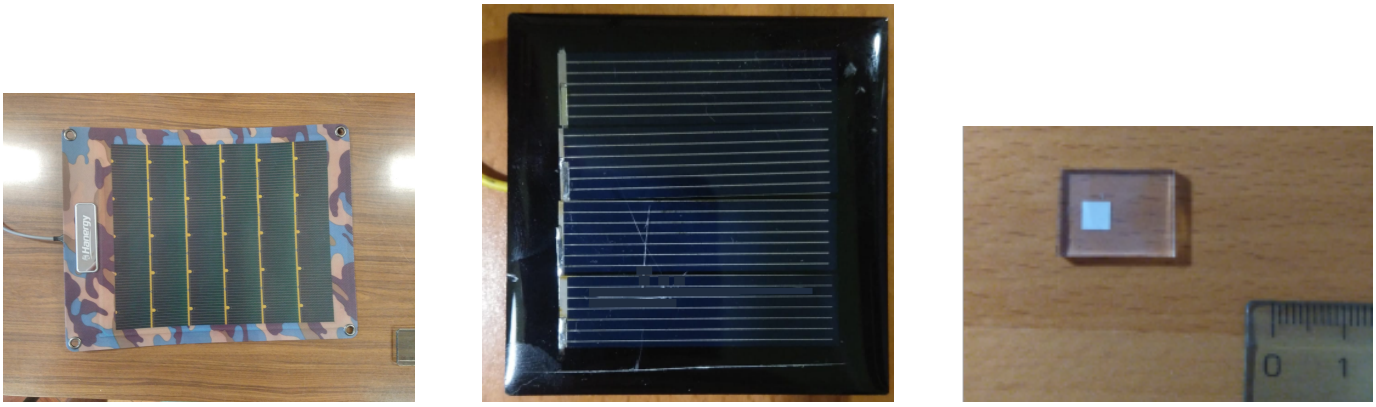

(a) Flexible CIGS solar panel. (b) Crystalline Silicon solar panel. (c) Dye-sensitized solar cell.

Figure 5.1: The three different panels to represent each solar cell material generation.

5.1 Preparation

To initiate the experiment, the equipment must obey the setup according to Figure 5.2.

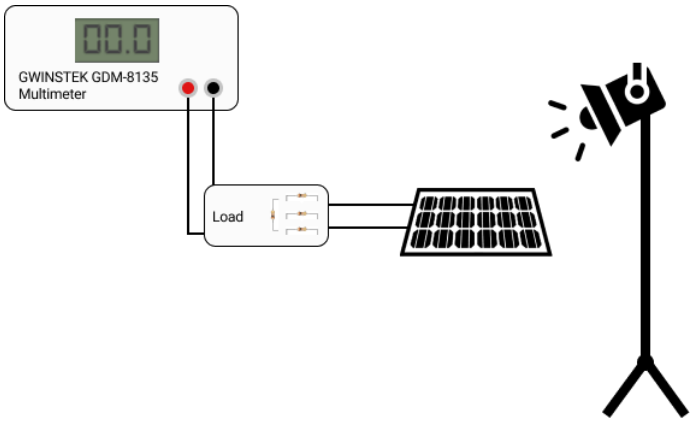

Figure 5.2: Schematic of the setup to be used during the experiment.

Firstly, to be able to register the output voltage of the solar cells the *GWINSTEK GDM-8135* multimeter was used. In front of the multimeter, there is a matrix of resistors. This matrix is the load to which the solar cell will connect and it's comprised of 100Ω and 51Ω resistors, connected in parallel and in series, varying the size of the load. To complete the necessary apparatus, the solar cells were positioned on top of the table and the light projector was set next to the cell. The final result is presented in Figure 5.3.

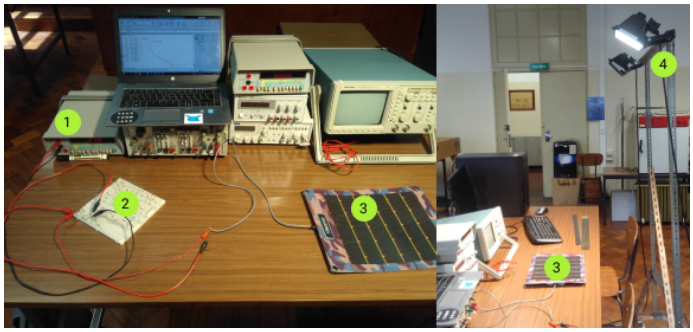

Figure 5.3: Setup of the experiment. 1) *GWINSTEK GDM-8135* multimeter; 2) Load (resistor matrix); 3) Solar cells; 4) Light projector

Before starting the experiment, it is of the up most importance to monitor the lighting conditions for both cells. Using an irradiance monitor, it was possible to maintain the irradiance at about $115W/m^2$ in average. This is commonly a low value of irradiance, but it was necessary to avoid any damage to the solar cells due to excessive heat. This can lead to possible tears and cracks of the cell, and when operating with CIGS, this avoidance is very important, due the possible release of toxic materials, such as cadmium. Therefore, the halogen projector was placed at a safe distance of 1m from the panels.

Afterwards, the resistor matrix was built in an order that could better define the extraction of data to plot the I(V) characteristic of the cells. The output voltage of the circuit was exported to MATLAB, to better produce the I(V) and P(V) curves.

Table 5.1: Properties of both the CIGS and Silicon solar cell

	Cell area (cm^2)	Irradiance (W/m^2)
c-silicon	16 (4×4)	115.4
CIGS	294.5 (19×15.5)	114.6

5.2 Experimental results

5.2.1 I(V) curves

The two solar cells were tested under the same conditions with the same equipment under total illumination of the projector, achieving the following I(V) characteristics, depicted in Figure 5.4 for Silicon and Figure 5.5 for CIGS.

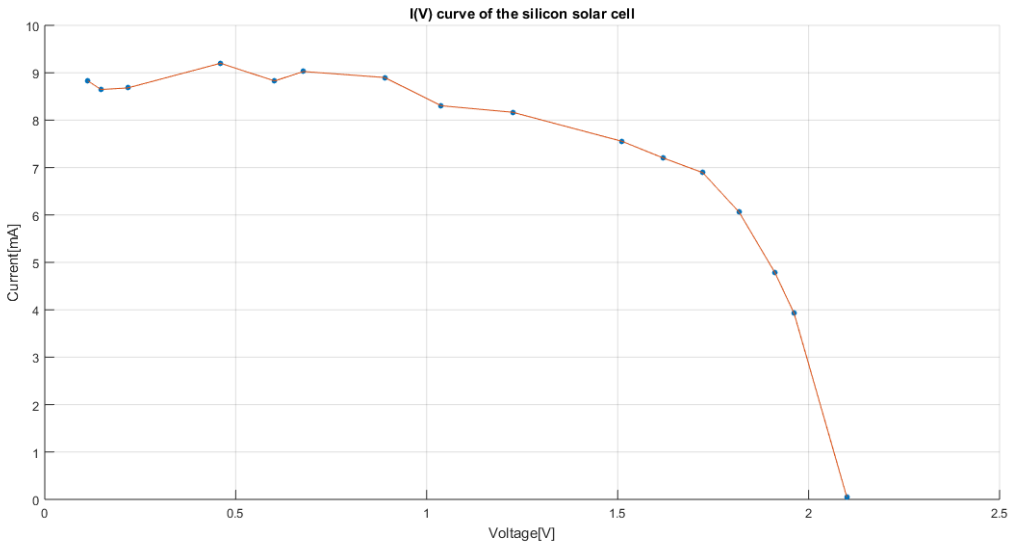

Figure 5.4: Obtained I(V) curve for Silicon solar cell with experimental results.

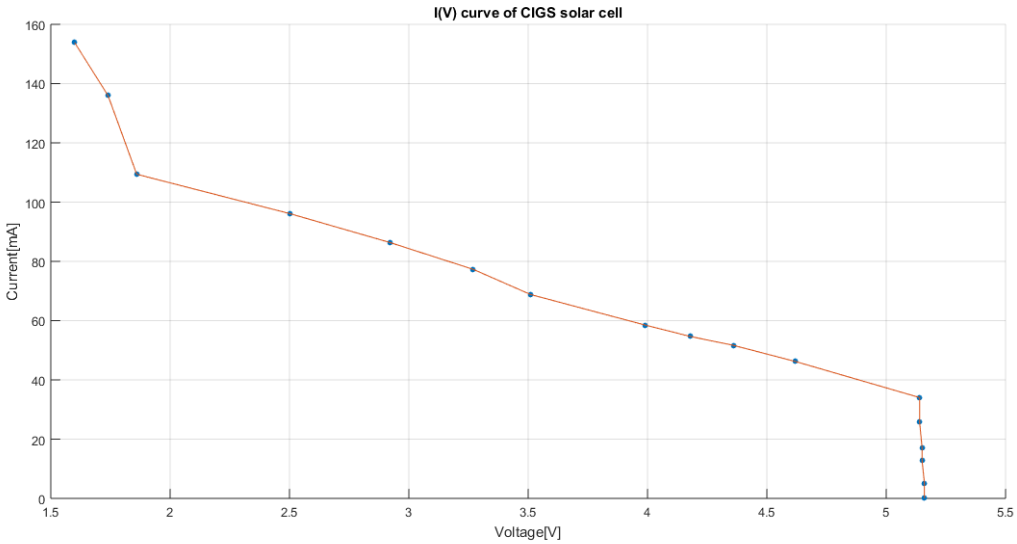

Figure 5.5: Obtained I(V) curve for CIGS solar cell with experimental results.

From Figure 5.4 it is possible to verify that the I(V) curve for silicon is very close to the ideal model of a solar cell, obeying Equation 2.2. The deviations from the ideal model comes from the possible shunt resistance, R_{sh} or series resistance, R_s that are generated by small imperfections of the layers or conduction losses of the connecting wires, resulting in small deviations from the ideal model.

On the other hand, Figure 5.5 shows that there is a clear difference between the CIGS I(V) curve and the ideal I(V) curve of a solar cell. The main deviation may come from the fact that it was seen previously that CIGS is heterojunction, composed by very different materials on different layers. This increases the possibility for the creation of small resistances that have a much more influential impact on the I(V) curve, than the silicon's homojunction.

Taking a more closer look at the CIGS I(V) characteristic, the following conclusions were withdrawn:

- **For** $5.16V$ **and** $5V$ the CIGS panel's current rapidly increases at huge slope, as it should be, comparing to the ideal model. The curve of the cell is a bit more abrupt than the ideal model, but it could caused by the heterojunction of different materials. This alludes to a possible internal low series resistance within the model, because the series resistance dictates the slope of this region, the higher the slope, the less influence will the series resistance, R_s, have on the circuit

- **From** $5V$ **to** $2V$ the current is steadily increasing, contradicting the very slow increase and stabilization of the current at the I_{SC}. Nevertheless this behaviour is not totally unrecognizable. When the shunt resistances of a solar cell are very low, there is an increase of the slope for this region, thereby enforcing the possibility of an internal shunt resistance within the CIGS solar cells.

- **From** $2V$ **to** $1.6V$ the slope increases drastically. At this point the resistance of the load is at its minimum value (10Ω). The only plausible explanation to this dramatic shift is given by M. Burgelman study on CIGS material. On his study, he proved the existence of inlayer resistances that were formed during the fabrication process which could behave as shunt resistances. This resistance is formed naturally during fabrication, however since the CIGS solar panel under analysis is flexible, the fabrication process must have been different from regular rigid thin-film solar cells. Therefore, the shunt resistance effect was amplified [33].

- **From** $1.6V$ **to** $0V$ there are no values shown, however with the previous conclusions, it is safe to assume that the linear behaviour would remain identical and to better represent these results a linear regression was considered to determine the value of the I_{SC} of the CIGS panel.

To compare both electrical properties of these solar cells, the effective area must be taken into consideration, since both cells have very distinctive sizes. Since it was not possible to determine directly the I_{SC} for the CIGS PV panel, as previously referred, a linear regression was made to better determine the exact value of I_{SC} per effective area.

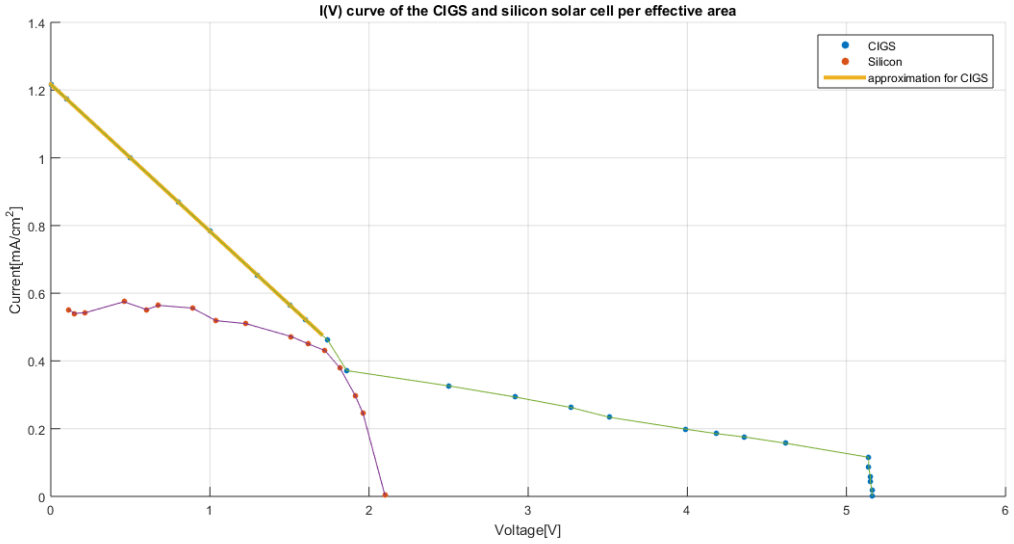

Figure 5.6: I(V) curve for Silicon and CIGS per effective area.

When determining the I_{SC} of a PV panel this value can be safely assumed if the resistance of the load is very low, in a quasi-short-circuit scenario. For the silicon PV panel this method was considered, since the minimum load resistance was 10Ω, resulting in a voltage of $0.113V$. Hence, $I_{SC}^{CIGS} = 0.552mA/cm^2$

Nevertheless, this approximation cannot be applied to the CIGS solar panel, because at the 10Ω mark, the output voltage was about $1.6V$, therefore the linear regression was applied, achieving the following, $I_{SC}^{Si} = 1.217mA/cm^2$.

After obtaining the I(V) characteristic for both solar panels, the P(V) characteristic was also obtained. As it was done for the I(V) curve, the power-voltage characteristic was calculated per effective area, to better compare both solar cells. Keep in mind that this value does not correspond to the current density of the solar cell. A misunderstanding may originate since both metrics are using the same units (mA/cm^2). If this metric corresponded to the solar cell's current density, then the whole PV panel would consist of just one very large solar cell with the same area as the panel, which is neither accurate nor true, because the solar panel is composed by a certain number of connected solar cells. The P(V) curve is illustrated in Figure 5.7 and the necessary results to later calculate the FF and the efficiency were registered on Table 5.2.

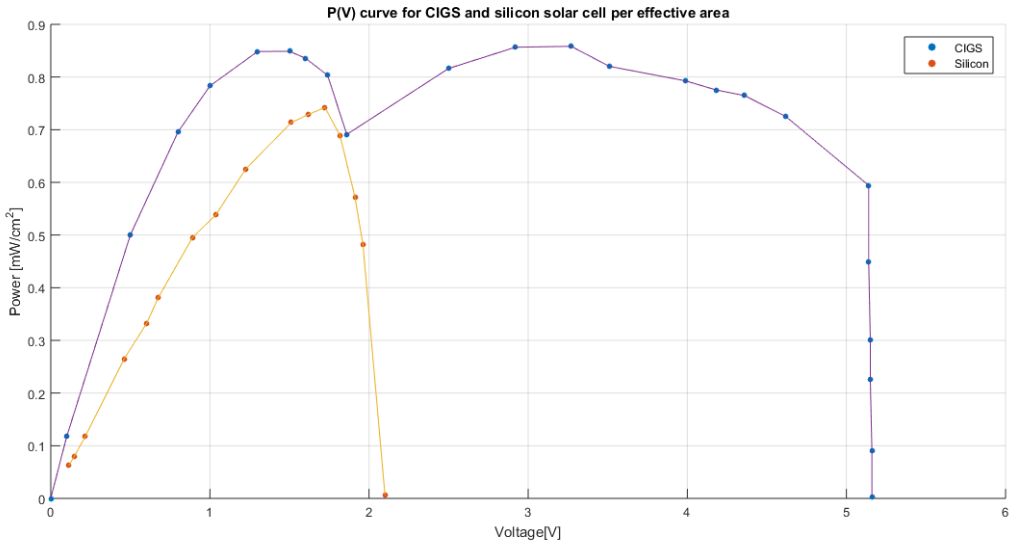

Figure 5.7: P(V) curve for Silicon and CIGS per effective area.

Table 5.2: Extracted electrical properties of the silicon and CIGS solar panels.

	$V_{OC}(V)$	$I_{SC}(mA/cm^2)$	$I_{max}(mA/cm^2)$	$V_{max}(V)$	$P_{max}(mW/cm^2)$
Silicon	2.10	0.552	0.4308	1.723	0.7422
CIGS	5.16	1.217	0.2625	3.27	0.8584

When analysing the Table 5.2, the highest V_{OC} and I_{SC} is registered on the CIGS solar panel. A possible explanation for this result could be the number of solar cells within the panel and how they are connected, in series or in parallel. By definition and assuming all solar cells of the panel are identical, solar cells connected in series present a higher V_{OC}, since the open-circuit voltage of the panel is the total sum of all the solar cells' V_{OC}. While, on the other hand, when the cells are connected in parallel, the V_{OC} is equal to the V_{OC} of just one cell, but the I_{SC} of the panel will be the sum of all the currents from each cell. This is fundamental basics of Kirchhoff's Current and Voltage laws, but applied in the solar cell environment.

With this definition in mind, the CIGS panel, may contain more solar cells connected in series than Silicon, which is not an improbable statement, as a result of the bigger size of the CIGS panel over the Silicon one, which is 18 times bigger, so not only are there more cells, but it is also possible that there are more connected in series than in the Silicon panel.

To calculate the fill factor, FF, and the efficiency, η, of the solar panel, Equations 2.7 2.8 respectively were taken into consideration, outputting the results observed in Table 5.3.

Table 5.3: Fill Factor

	FF (%)	η (%)
Silicon	64.03	6.43
CIGS	13.67	7.44

The crystalline Silicon solar panel registered a 6.43% efficiency with a fill factor of 64.03%. Despite the low efficiency,

the obtained fill factor is very high, which is good. Moreover, the CIGS flexible panel achieved a a higher efficiency than Silicon, however its fill factor is drastically low, since the "squareness" of the CIGS I(V) curve is far from the ideal one.

5.2.2 Light absorption

In addition to the electrical analysis of the solar panels, the absorption of each material was also checked. To create a link between the simulation results and the experiment, for this section of the study it was proposed the comparison of the emitting spectrum from the light projector with the responsivity spectrum of Chapter 4.

The lighting projector used in this section is the Ersetze Jede Gebrochene Schutzscheibe R7s 500W max, composed of an halogen light bulb type. The emission spectrum for the lamp is presented in Figure 5.8, on a normalized scale for just 1 light bulb. As it can be seen, the projector has a very low emission rate around the UV regions of the spectrum, but around the $400nm$ the emission increases at a faster pace through the visible regions and reaches its maximum around the $900nm$. The emission spectrum is normalized for just one type of light bulb, if there were to use the same light bulb at twice the power, it would be the equivalent of duplicating this graph.[47]

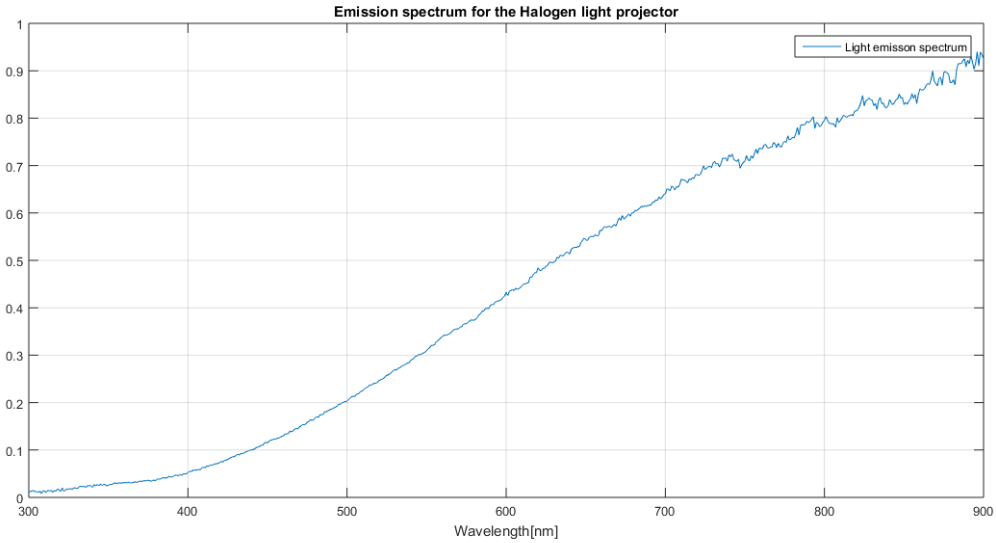

Figure 5.8: Emission spectrum for the halogen light projector.[47]

Since the only solar cells that were used in this experiment were the CIGS and crystalline silicon ones, only the absorption's of these two materials will be considered. In case of CIGS, three of the five CIGS types used in this study were considered: CIS, CGS and CIGS-45. These three compounds were selected in order to represent the three possible corner cases of gallium concentration in CIGS.

The connection between the simulated responsivity with the light emission spectrum, can allude to the better understanding of the performance of the solar panels.

As it was seen previously, silicon's efficiency presented to be lower than the CIGS panel, but nonetheless its FF proved that the main problem was related to the area of the cell.

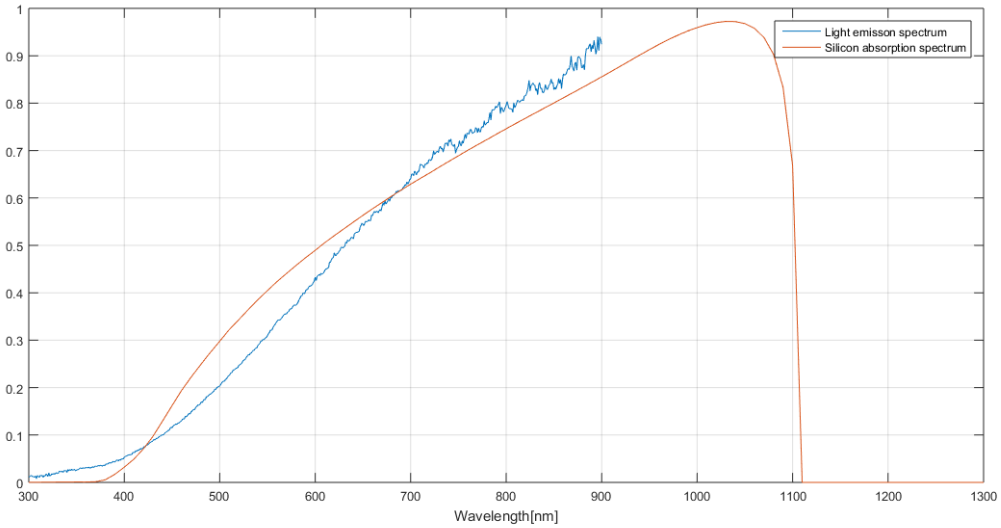

Figure 5.9: Emission spectrum for the halogen light projector.

After observing Figure 5.9, it is clear to see that silicon's responsivity covers various regions of the light spectrum.

- **Between the** $300nm$ **and** $380nm$ silicon does not absorb any of the incident light, since this corresponds to the UV region. Even if it was inside the absorption spectrum of silicon, the amount of irradiated light would be very little, absorbing in both cases no UV radiation whatsoever.
- **For the** $400nm$ **and the** $700nm$ silicon's responsivity starts increasing at a fast pace, even surpassing the light projector's irradiation. The light emission also increases, but not as steep as the silicon's responsivity at first. Nonetheless, radiation absorbed will be absorbed by the solar cell, since both functions are increasing and also because silicon has a very high current generation at this gap.
- **From** $700nm$ **to** $900nm$ the light emission reaches its peak. Despite the silicon's responsivity peak at $1040nm$, the responsivity still circles the 70% all the way up to 90% around the red and IR region.

This shows how high the current can be generated in the silicon material for this particular light. However, the experimental results don't share the same statement, because the CIGS I_{SC} per area is higher than Silicon's. The main reason behind this claim, lies on the area of the solar panel. Given that the area of the silicon solar cell is very small and the distance between the panel and the light source was about 1 meter, most of the projector's light will be not be entirely directed at the solar panel, meaning it will mostly be dispersed onto the table, rather than the solar panel. Although area is the main justification, in other cases reflection on the panels's surface can also have a huge negative influence in the photocurrent generation, but in this case, area was a more important factor.

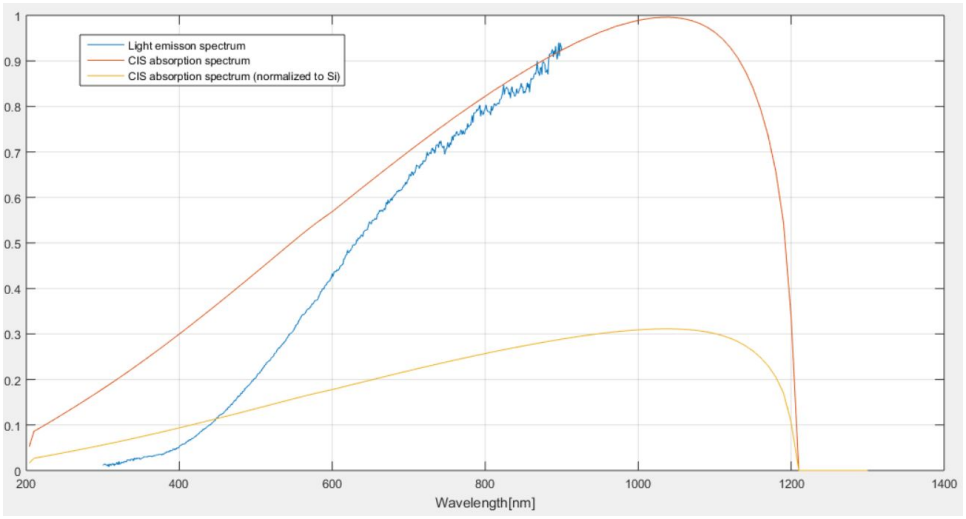

(a) Comparison of the light emission spectrum with CIS responsivity.

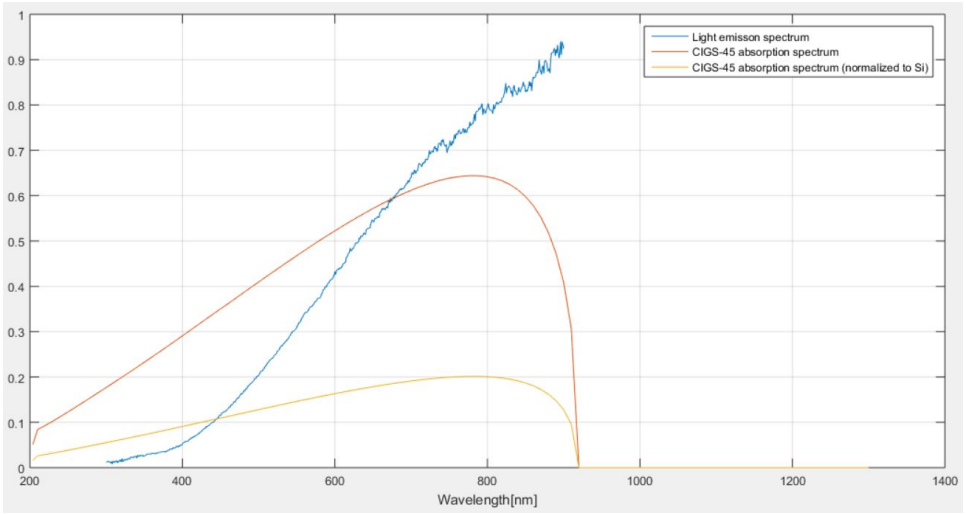

(b) Comparison of the light emission spectrum with CIGS45 responsivity.

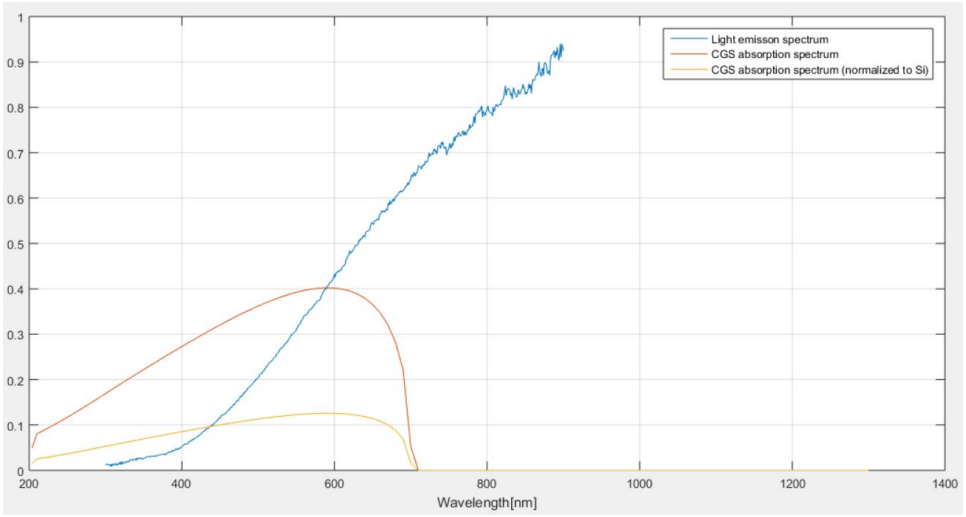

(c) Comparison of the light emission spectrum with CGS responsivity.

Figure 5.10: The three different responsivities of CIGS, for different percentages of gallium.

Looking at Figure 5.10, it is possible to once again verify the impact of gallium on CIGS responsivity range.

This effect will impact the amount of current that will be generated through the solar panel. There are two types of absorption spectrum illustrated. The orange one, is normalized at the highest values registered for the CIGS responsivity, providing a better comparison between the gallium concentration, while the yellow one is normalized at silicon's maximum responsivity, which allows the comparison between these two materials.

Analysing each spectrum for different types of radiation, it is possible to state the following:

- **At the** $200nm$ **to** $400nm$ region of the graph, it is possible to verify that little to zero radiation will be generated into current, due to the lack of light emission at that region, regardless of the concentration of gallium.
- **From the** $450nm$ **to** $900nm$ the light emission starts increasing and so does the CIGS responsivity. At this mark, the gallium concentration comes into action. Analysing for CGS first, the cell starts producing current at $710nm$, this means that only the visible spectrum will be absorbed by the cell and transformed into current. This means that the generation of current from the light will be very small, since most of its highest wavelengths will pass through the cell or will be reflected, as the wavelengths that are encompassed in the responsivity of CGS, will produce current equivalent to 40% of CIS maximum. For the CIS solar cell the highest peak in responsivity is located on $1060nm$, which implies that no light will reach the maximum current generation point. However, on this window, the maximum emission of the light projector is very close to the maximum of absorption, which means that more current will be produced. The generated current will be high, but not as high as if it compared to silicon, since it's much lower. The CIGS-45 cell is the middle ground between the CGS and the CIS, since its responsivity peak is around 780nm about 60% of the CIS maximum and stops absorbing at $920nm$. This material can absorb throughout the whole emission spectrum of light, making it a good candidate for the assumption of the type of CIGS material.

Through this analysis, it is possible to determine the corner cases of the gallium concentration in the CIGS panel. According to the experimental results, the CIGS panel achieved a higher I_{SC} than silicon, despite being calculated by linearization, instead of experimentally.

Although, the area for the CIGS panel was much higher, meaning most of the radiation was from the projector was dispersed onto the table. It is possible to conclude that the used solar panel was not of the type CGS, since the output current should have been much smaller. Nonetheless it is still uncertain whether to determine the precise amount of gallium inside the panel, it would be plausible to assume that the CIGS panel is comprised between the CIGS-45 and the CIS solar cell type, even though the designed model of CIGS is mainly depicted for the absorber layer.

In her study, Isabela has shown that CIS can absorb 60% more IR radiation than the CGS solar cells (Figure 5.11) , which confirms the previous statement [7]. Since the light projector had a higher emission in the IR region, it is possible to assume that the solar panel contained fewer concentrations of gallium.

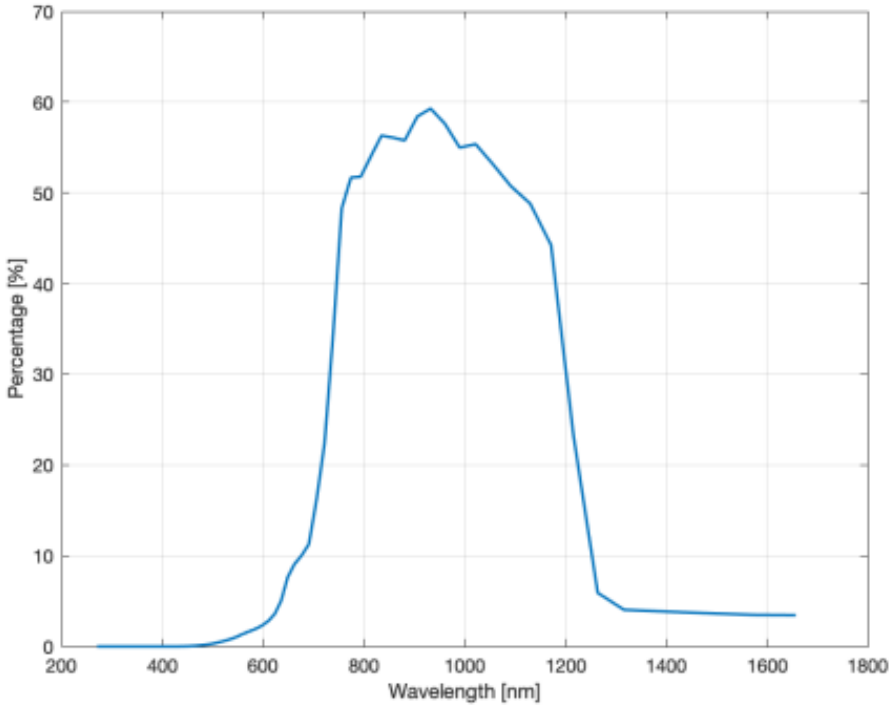

Figure 5.11: Percentage difference in absorption between CIS and CGS solar cells.[7]

5.2.3 V_{OC} analysis

In this portion of the chapter, the attention is directed mainly at the V_{OC} of the solar panels. Given the different characteristics and properties of each solar cell, the objective with this analysis would be to establish a correlation between one of the PV cell's performance indicators, the V_{OC}, with internal properties of the material at hand.

T. Kirchartz and U. Rau in their study have investigated different models that use either external or internal parameters to allow the calculation of J-V Curves, J_{SC}, V_{OC} and subsequently the efficiency and FF. External properties of the solar cell are said to be the parameters that are looked from the outside of the cell, describing it essentially using external quantum efficiencies and absorptance. On the other hand, internal parameters such as the absorption coefficient, mobility, lifetime and internal quantum efficiency can be included in Drift-Diffusion models which allow the calculation of the referred parameters of the solar cell [24]. The researchers in this article, use Equation 5.1 to relate the material's band gap with the V_{OC}, but in the scenario where the solar cell's absorber layer is fully depleted.

$$V_{OC} = 2kT \cdot \ln\left(\frac{J_{SC}}{qd\frac{\sqrt{N_C N_V}}{2\tau}\exp\left(\frac{-E_g}{2kT}\right)} + 1\right) \tag{5.1}$$

Where,

$$qd\frac{\sqrt{N_C N_V}}{2\tau}\exp\left(\frac{-E_g}{2kT}\right) = J_0 \tag{5.2}$$

This means that the relationship between the V_{OC} and the band gap comes from the saturation of the current density, J_0. This is perfectly acceptable since the saturation current is created by a very few amount of (thermally) excited electrons with higher energy than the band gap, that generate electron-hole pairs, therefore originating a very small electrical current. It is also important to notice that the ideality factor in this scenario is consider to be 2.

In order to use this formula, some assumptions had to be made:

- **Assumption 1** - For starters, to use this equation, it was assumed that the absorber layer of the solar cell was fully depleted.
- **Assumption 2** - Secondly, the internal values of the materials that were used are originated from the simulations.
- **Assumption 3** - Lastly, it was used the obtained I_{SC} per effective area from the experimental results to replace the necessary short circuit current density. As said previously, this assumption implies that the solar panels are composed of only one single solar cell, with the same area as the whole panel.

Computing Equation 5.1 with the necessary values, it is possible to retrieve the following open-circuit voltages, depicted in Table 5.4.

Table 5.4: Calculated values for V_{OC} using the equation in T. Kirchartz and U. Rau article.[24]

Materials	**Silicon**	**CIS**	**CIGS-31**	**CIGS-45**	**CIGS-66**	**CGS**
V_{OC}	0.704	0.512	0.712	0.832	0.972	1.252

As it is possible to verify, as the gallium concentration increases in CIGS, so does the V_{OC}. The main reason behind this rise is a result of the increasing band gap, since the gallium concentration influences the band gap of CIGS.

The experimental values of the V_{OC} are about $5.16V$ and $2.10V$ for the CIGS and silicon solar panel respectively, while the highest theoretical value for V_{OC} is $1.252V$ and $0.704V$ for the CIGS and silicon solar panels respectively.

This means, it is not possible for the the solar panel to represented by just one solar cell and there must be a series of n solar cells, in order to produce the experimental values for V_{OC}, which is why assumption number 3 erroneous and didn't entirely represent the actual reality, thus not been taken into consideration in the previous sections of the experiments.

However, it is still possible to estimate the number of solar cells that each solar cell has. Once again, assuming that all the solar cells are equal and connected in series, Table 5.5 will depict the new estimated values of V_{OC}.

Table 5.5: New estimated values of V_{OC} for different numbers of solar cells connected in series

Materials	**Silicon**	**CIS**	**CIGS-31**	**CIGS-45**	**CIGS-66**	**CGS**
V_{OC}	0.704	0.512	0.712	0.832	0.972	1.252
Estimated # of cells	3	10	7	6	5	4
Estimated V_{OC}	2.112	5.12	4.984	4.992	4.86	5.008
Experimental V_{OC}	2.12	5.16				

After analysing the table above, it is possible to approximately determine the obtained V_{OC} comparing it with the experimental values. For silicon it's possible to see that 3 solar cells generate the same voltage as the entire panel.

For CIGS it is possible to check that the number of required cells decreases every time the gallium concentration is increased, since the voltage gets higher. However, if the solar cells were all in series it is possible to assume that the concentration of the CIGS is panel would be mainly indium, but it is a statement that cannot be entirely certified.

Chapter 6: SEM Analysis

SEM stands for Scanning Electron Microscope. This type of microscope is used for observations of surfaces at great detail, using electrons instead of light to form an image from a sample.

This specimen (or sample) when irradiated with a fine electron beam, secondary electrons are emitted from the specimen's surface, hence forming a 2D image as if it was seen from the naked eye.

When electrons from the beam enter the specimen, the electrons are dispersed within its material and gradually lose their energy, until they are eventually absorbed by the specimen itself. Afterwards, secondary electrons are produced from the emission of the valence electrons of the constituent atoms in the specimen. Since their energy is very small, those generated at a deep region are quickly absorbed by the sample.

When looking at a SEM image, it is possible to detect a lot of detail of the constituent materials as well as a sense of depth. This has to do with brightness of the crystal surface, which is caused by the incidence angle of the electron beam. It occurs as a result of an anomalous contrast once the specimen is electrically charged.

In addition, it is also possible to detect the elements that compose the sample. The SEM can perform an Energy-Dispersive (EDS) analysis, using an x-ray radiation to excite the electrons and since each element of the periodic table has different energy levels, it is possible to associate each excited electron to an element, recording as well the percentage of that element in the specimen.

To better comprehend and to learn about the composition of the studied solar cells, a SEM analysis was conducted. This type of study allows the better understanding of the solar cells at hand. For example in the case of the CIGS solar cell, it is possible to verify the percentage of Ga within the layers or to learn how the layers are truly distributed.

To perform an analysis, the samples must be submitted into a preparation procedure beforehand. This procedure, requires the deposition of some metals and other chemical compounds on top of the surface that will be inspected by the SEM. In order to perform the chemical deposition, the orientation of the analysis must be defined in advance. Since the solar cells' layers are seen from a transversal point of view, the specimen must be prepared from this orientation, otherwise it the obtained images correspond to all of the top layer of the solar cells.

Due to this lack of knowledge, it was only possible to perform an EDS analysis to the top layer of the solar cell, since the samples were prepared with the wrong orientation. The experiment had to be later repeated, in order to capture the correct SEM images. However, the EDS analysis wasn't possible to perform on the second try.

Starting with the CIGS solar cell, has it can be seen in Figure 6.2, the cell contains a high percentage of Fluorine, roughly 64% and 36% Carbon at a 3.9μm depth. This doesn't match with any of the CIGS layers that were previously specified in the study. Although, the high amount of Fluorine may indicate that the the first layer can be made from FTO - Flurine Tin Oxide - a material usually used in Perovskite solar cells as a substrate, despite no traces of tin were found.

On the second trial of the analysis, the SEM images were as they should have been expected, as it can be seen in Figure 6.1. In this SEM image is not fully clear how many layers there are, but it is clearly possible to see the top encapsulating layer that appears to have a fabric-like texture, as it can be seen by the amount of fibers.

The bands that seem to follow up the fabric layer are not entirely distinguishable, but it is possible that the top layer of the image may correspond either to an encapsulation material that is different from the fiber, or it could be a flexible substrate of the cell. To better comprehend the types of each layer, an EDS analysis is required for each layer to determine which material is which.

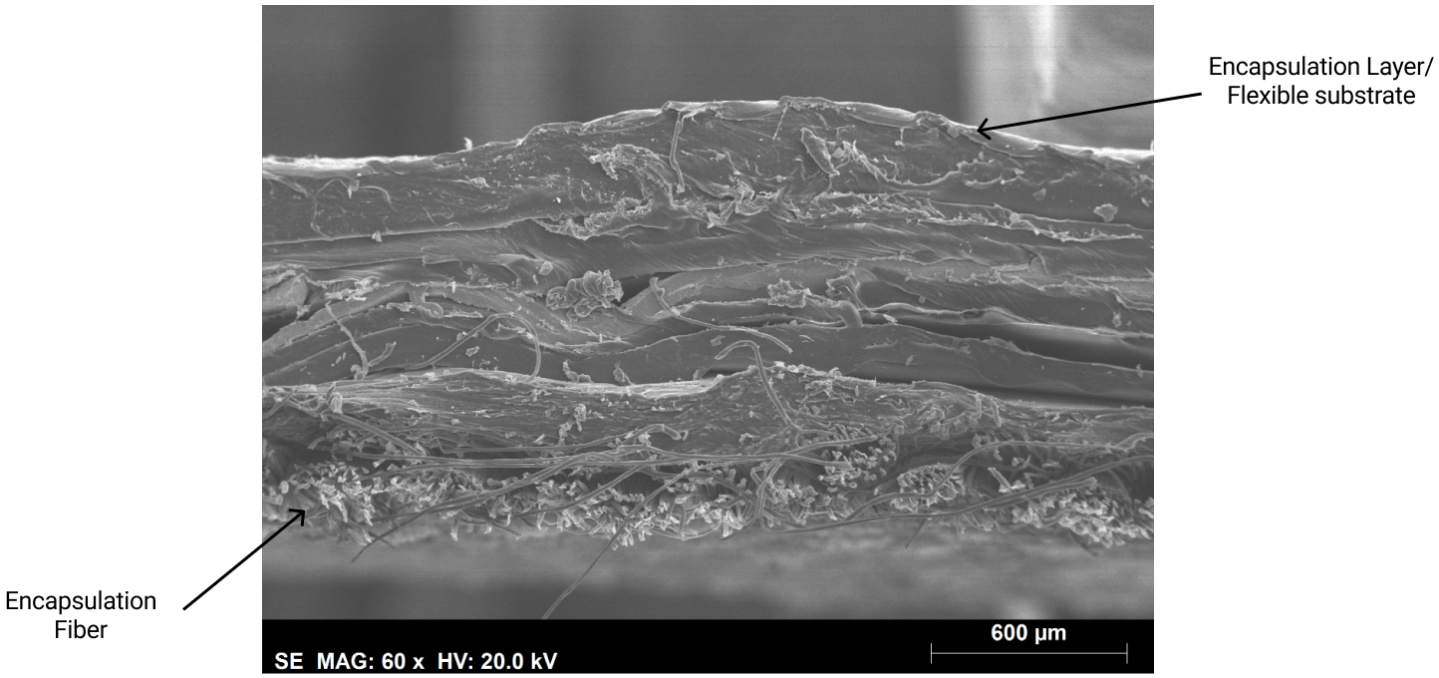

Figure 6.1: Cross-sectional SEM image from the CIGS material, with some suggestions of the definition of each layer. Note that the solar panel is upsidedown.

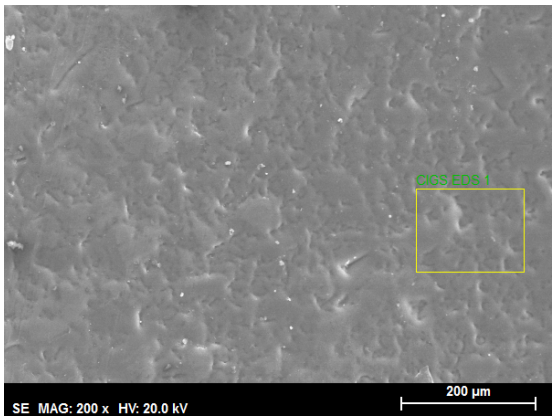

(a) CIGS' top layer SEM image. Yellow square represents the area where the percentage of elements was measured

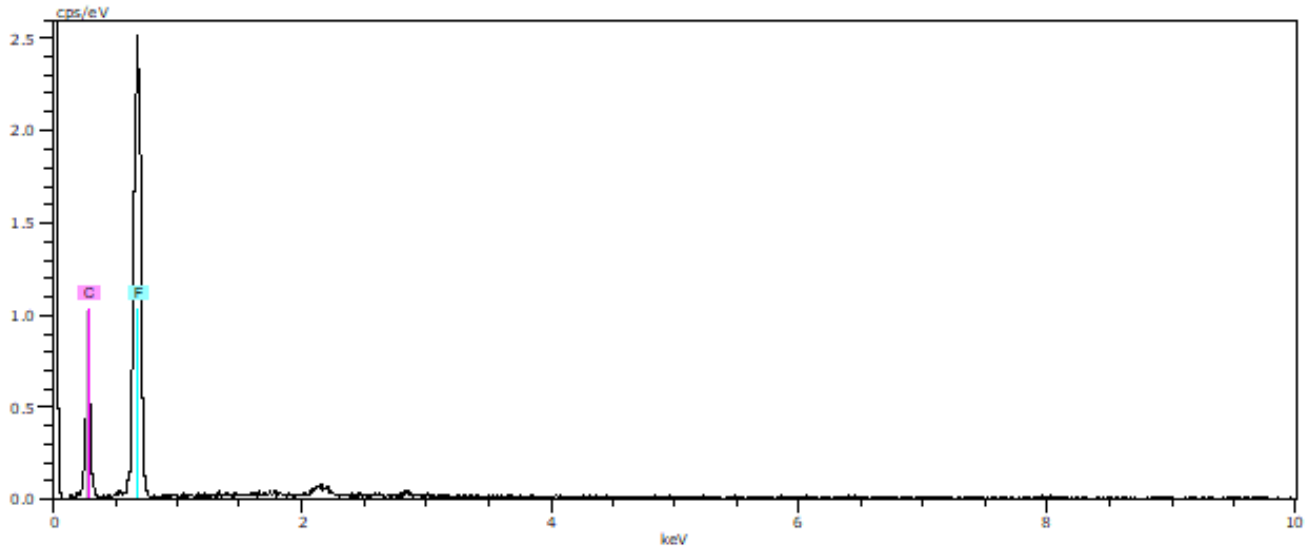

(b) Qualitative EDS analysis from the CIGS sample. Revealing only Carbon and Fluorine as the main constituents of the encapsulation material.

El	AN	Series	unn. C [wt.%]	norm. C [wt.%]	Atom. C [at.%]	Error (1 Sigma) [wt.%]
F	9	K-series	63.79	63.79	52.69	8.71
C	6	K-series	36.21	36.21	47.31	6.47
		Total:	100.00	100.00	100.00	

(c) Results of the quantitative EDS analysis, featuring different types of concentrations (normal and atomic).

Figure 6.2: SEM analysis results for CIGS solar cell at a $3,9\mu m$ depth

The next material to be analyzed was the silicon solar cell and this time it was clearly possible to check that the chemical compounds were of the outer encapsulation layer of the cell rather than the silicon layer. This statement can be checked in Figure 6.5, since no amount of silicon was detected, while on the other hand, large traces of Carbon and Oxygen were discovered, along with some small amounts of Chlorine.

On the other hand, when the second analysis was conducted it was possible to clearly detect the layers of the silicon solar cell, depicted on Figure 6.3. With the aid of Figure 6.4 from a silicon solar cell study, it is possible to safely assume some of layers for the used solar cell.

At the top, there is the possible TCO (transparent conductive oxide) of the solar cell. Although there is no certainty on the type of material that composes this layer, but it safe to say that is an oxide of some sort, due to the high presence of oxygen atoms in the top layer.

After the TCO, there is a $225\mu m$ crystalline silicon layer. It's not possible to determine whether it is a P-N or PIN type silicon, but thanks to the Figure 6.4 it is possible to see that the silicon layer is one of the largest in-layers. The rest of the layers follow the same order. There is a possible Metal/TCO contact with $37.5\mu m$ thickness, followed by a $65.5\mu m$ dieletric coating layer, all built on top of the substrate that can be made from ceramic tile. However, the EDS analysis would come a long way in supporting these assumptions.

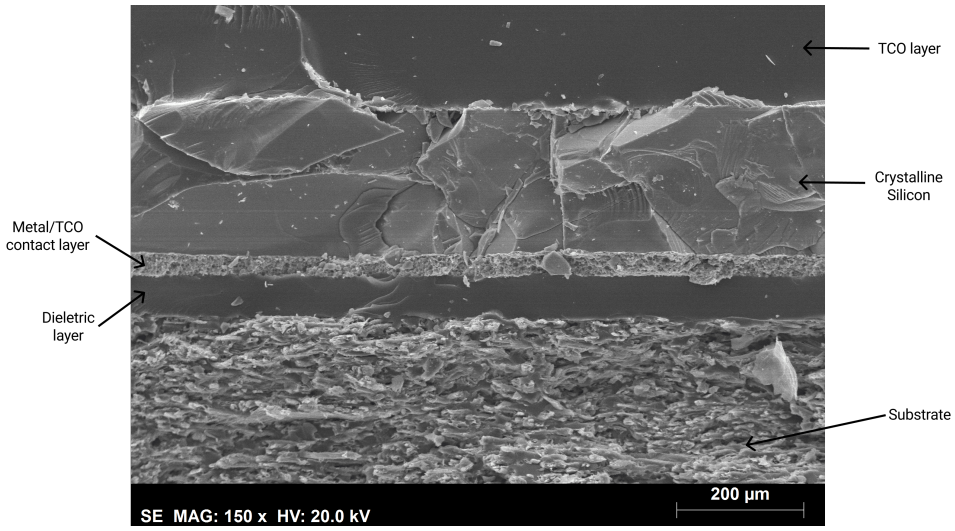

Figure 6.3: Cross-sectional SEM image from the silicon cell. It is possible to tell apart each layer of the cell as presented on the image.

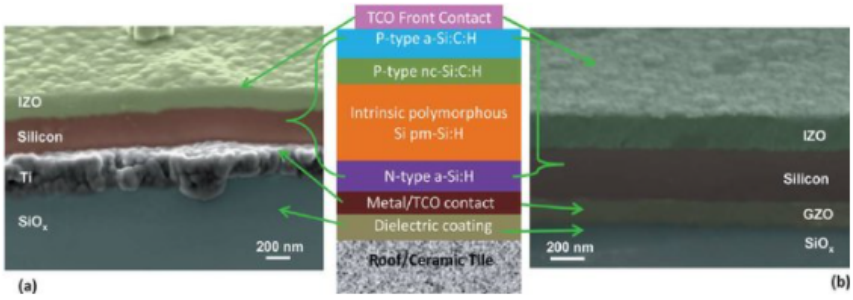

Figure 6.4: Theoretical constitution of silicon solar cell with two different contact layers a) Metal (Titanium) b) GZO (Gallium dopped zinc oxide). [54]

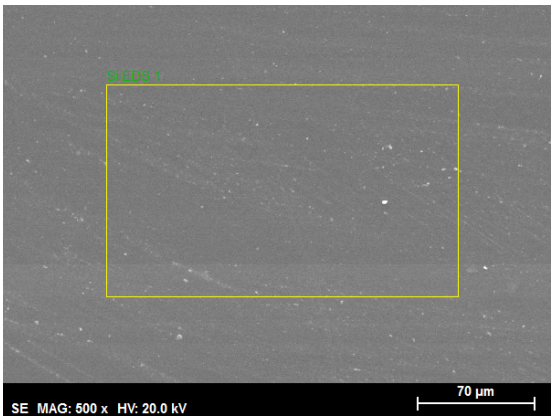

(a) Silicon's top layer SEM image. Yellow square represents the area where the percentage of elements was measured

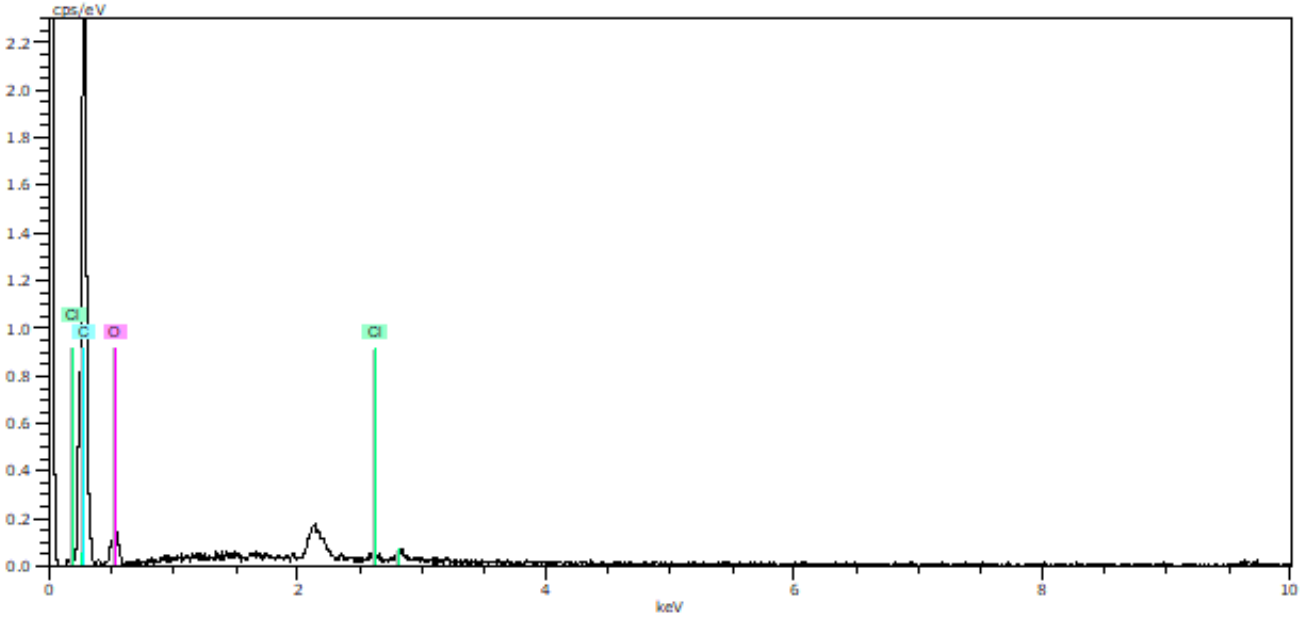

(b) Qualitative EDS analysis from the Silicon solar cell sample. Revealing only Oxigen and Carbon as the main constituents of the encapsulation material.

El	AN	Series	unn. C [wt.%]	norm. C [wt.%]	Atom. C [at.%]	Error (1 Sigma) [wt.%]
C	6	K-series	80.13	80.13	84.45	11.17
O	8	K-series	19.48	19.48	15.41	4.65
Cl	17	K-series	0.40	0.40	0.14	0.06
		Total:	100.00	100.00	100.00	

(c) Results of the quantitative EDS analysis, featuring different types of concentrations (normal and atomic).

Figure 6.5: SEM analysis results for Silicon solar cell at a $3,4\mu m$ depth.

Finally the last material to be submitted into the SEM analysis was the DSSC. This solar cell was the only one that it could be possible to extract the first layer accurately, because this cell was mainly encapsulated in glass, which can be proven in Figure 6.8. The large amounts of Silicon and Oxigen, mixed with some traces of Sodium and Calcium are commonly found in glass substrates.

When running the DSSC solar cell under the SEM device at a cross-section, it is possible to detect a small layer that could correspond to the electrode of the solar cell, as seen in Figure 6.6. There have been a few DSSC solar cells that have been built with a small layer of graphene, between the substrate and the TiO_2, which provide some mechanical stability as well as a possible increase in electron mobility [12]. Once Figure 6.6 is compared with another SEM analysis it is possible to say that the small irregularities could be a very thin graphene layer. Above the graphene it is possible to find a compact layer of TiO_2, and it is also possible to assume the irregular spheres throughout the top of the electrode may be TiO_2 (porous) connected to the dye. However, to be certain of these claims, the EDS analysis had to be taken into consideration.

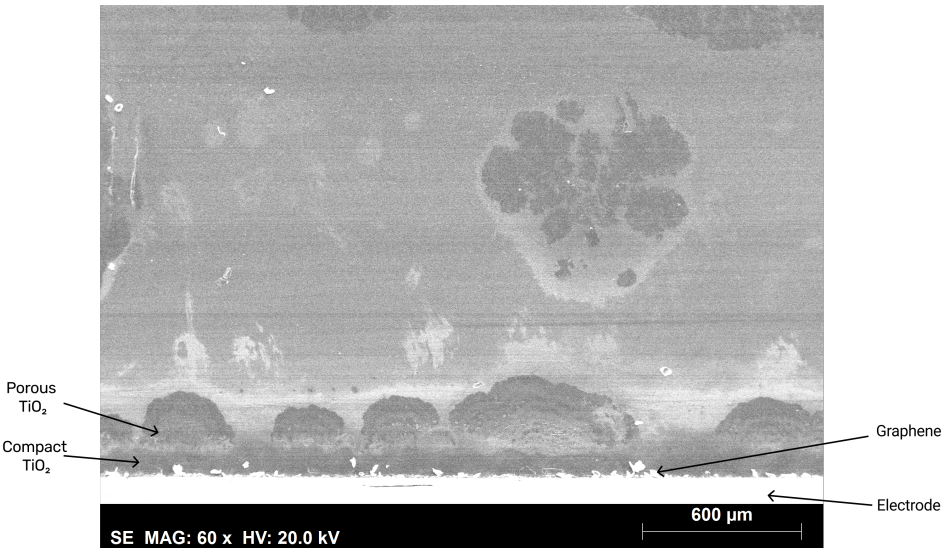

Figure 6.6: Cross-sectional SEM image from the DSSC, with some suggestions of the definition of each layer.

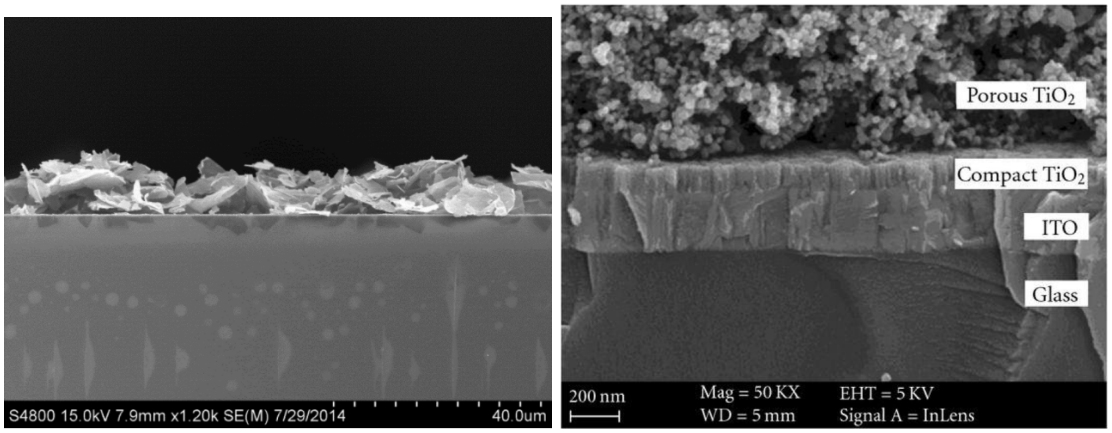

(a) Cross-section SEM image of the graphene flakes on top of the ITO substrate. [12]

(b) SEM cross-section image of photoanode with compact layer. [13]

Figure 6.7: SEM analysis from different studies, to verify the layer assumptions.

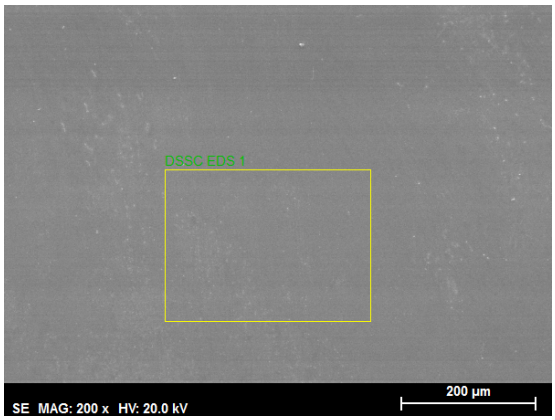

(a) DSSC's top layer SEM image. Yellow square represents the area where the percentage of elements was measured

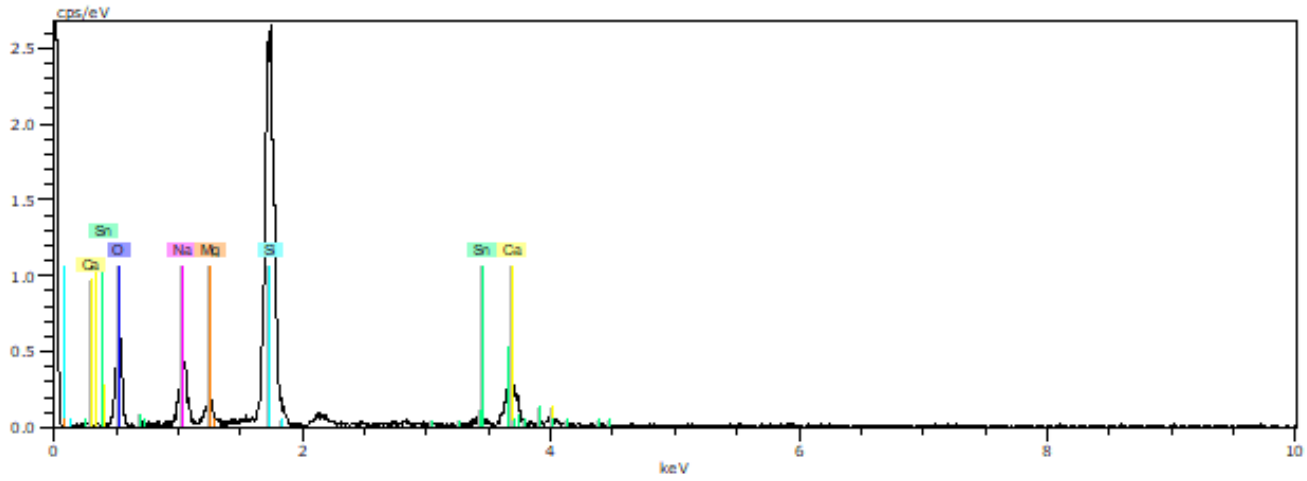

(b) EDS analysis from the DSSC sample. The DSSC was encapsulated in glass, which can be explained by the the types of materials detected in the spectrum.

El	AN	Series	unn. C [wt.%]	norm. C [wt.%]	Atom. C [at.%]	Error (1 Sigma) [wt.%]
O	8	K-series	35.72	36.99	52.05	7.30
Si	14	K-series	34.88	36.13	28.96	1.59
Na	11	K-series	9.92	10.27	10.06	0.80
Ca	20	K-series	9.11	9.44	5.30	0.41
Mg	12	K-series	2.99	3.10	2.87	0.28
Sn	50	L-series	3.92	4.06	0.77	0.26
		Total:	96.54	100.00	100.00	

(c) Results of the quantitative EDS analysis, featuring different types of concentrations (normal and atomic).

Figure 6.8: SEM analysis results for the DSSC at a $4,3\mu m$ depth.

Chapter 7: Conclusions and Future Work

7.1 Conclusion

The main goal of this dissertation was to perform a comparative study between different types of solar cells, through an electrical point of view. A model for a 2D solar cell was completed using a finite element tool, which simulated the behaviour of a semiconductor layer absorbing a user-defined radiation, to better understand the solar cells perfomance. In addition to the model, it was also performed a physical experiment in the laboratory, which could indicate the performance of the solar cells under a real scenario.

The second chapter captures some of the equations that were used in the simulation and in the determination of some electrical properties and metrics to define the perfomance of the solar cell. It also a brief explanation of the basic foundations of the solar cell and p-n junctions.

On the 3rd chapter of this dissertation it was possible to perform an analysis of the state-of-art for each technology and the advancements that were made in this sector. Representing the 1st generation of materials there is the silicon solar cell, the most common and dominating PV technology in the market. Nowadays, the c-Si is the most common used material for the development of PV panels at commercial scale, since its production prices got very cheap due to the increase of electronic devices which use silicon as its main material to design micro transistors, therefore increasing the demand of silicon production, thus lowering the price. Nonetheless, thin-film technologies came around as an alternative to silicon solar cells, due to their very thin and lightweight panels, with adjustable band gaps (through heterojunctions) and diversifying the PV industry, for more versatile applications, that ordinary c-Si couldn't handle, such as the CIGS material. Finally, the 3rd generation is mentioned. This generation was mainly inspired by the photosynthesis phenomenon, more focused on the incorporation of organic materials into the solar cell industry, setting themselves apart in the flexible solar cell industry. The first ones to come about were the DSSC, but to this date hybrid Perovskite detains the efficiency record, however still resorting to hazardous materials such as lead. What is promising the thin-film market is the possibility of creating flexible solar cells, which can later adopt a R2R production, which can facilitate the jump into mass production. It is also important to know, that these types of material are all taken into consideration when they reach their end-of-life cycle, since most of the hazadous materials are carefully removed from the solar cells for refurbishing purposes.

On Chapter 4, the simulation of the solar cells was initiated. Firstly, the model at hand was designed and simulated in *COMSOL Multiphysics*, a Finite Element Tool that allows the simulation of complex physical phenomena, approximating the models as close as possible to reality. The model that was used during this chapter was PIN structure model based on a 2D sample model of a GaAs PIN photodiode from the application library from *COMSOL Multiphysics*, which was altered to behave as a solar cell, since it is the same device just operating at different a bias. The PIN model is quite different than an ordinary p-n junction solar cell, since the PIN model is comprised by an extra intrinsic layer between the p and the n layers, with the goal of providing a higher depletion region, which can minimize the recombination of the minority carriers. During this chapter 3 materials were studied: Silicon, Gallium Arsenide and CIGS. It is important to keep in mind that the CIGS solar cell is composed of several layers and in this case it was

only considered the absorber layer, which corresponds to the copper indium gallium selenide material, CIGS. One of the assumptions, that was afterwards tested, was to consider CIGS as a PIN structure, when in reality it is considered a p-type heterojunction. To minimize the error, the n-layer of the PIN module was doped according to the solar cell's buffer layer, this way it was possible to simulate the contact with the n-layer. In addition, the CIGS solar cell also has some of its electrical properties that are gallium dependent, which consequently will lead into a deeper study of the affects that gallium has on the CIGS solar cell.

Firstly, to validate the model at use, the responsivity of the solar cell was simulated, comparing them with theoretical responsivity curves. The obtained results matched the same shape and absorbed closely in the same range as the theoretical curves, but the current that was generated was very lower than the theoretical curves. A plausible justification would be the area of which the solar cell was designed, because it was very small (around the μA). When evaluating the CIGS responsivity, it was much lower than expected, but since only the absorber layer was considered it could be a possible explanation to this discrepancy. It was also possible to check a decrease in the responsivity range of the solar cell as the gallium concentration was increased.

Next, the I(P) curves of the solar cell were analysed for each material and for different wavelengths, providing a better information of the relationship between incident power and current. This analysis had the goal of capturing changes in the linear behaviour between incident power and the generated current, so to better understand this, the *polyfit* function in *MATLAB* was used, in order to extract the polynomial expression that best fitted the data. Silicon and GaAs proved that first generation materials (homojunctions) have a linear relationship with between current and power, but for CIGS (an heterojunction) proved that the equation that best fitted the output data was a 3rd degree polynomial expression. However, this non-linearity only proved to be true for regions other than the UV, where it remained linear, regardless the concentration of Ga.

Chapter 5 was more focused on the real-life scenario. Here, it was performed the extraction of the I(V) curves and efficiency for different solar panels. Afterwards, the light absorption of each panel was estimated with the help of the simulated responsivities. Three solar panels were used in the laboratory, each one of them with the goal of representing each technology, however since DSSC cells were had no contacts to measure its voltage it was not possible to draw any conclusions from this solar cell. Nevertheless, the silicon and CIGS panel were able to produce their I(V) characteristic and it was possible to check that CIGS was the cell that output the highest V_{OC}, I_{SC} per area and efficiency, but it registered a poor FF. The main reason for this performance, had to do with the internal parasitic resistances within the solar cell that originate during the production process or are from the material's nature. The silicon panel on the other hand, achieved good results, and the main reason for the results are not higher than CIGS, it's because the silicon panel was too small. If the cell had a few more centimeters, more cells could have been connected, increasing its I(V) curve and efficiency.

The second experiment was based on the projector's light emission spectrum and the main goal was to estimate how much of the light was absorbed by the solar panels, given the responsivity for each solar cell obtained in the previous chapter. Here it was possible to verify that the main source of generated current originated from the red and IR regions of the light spectrum, however some visible radiation could have also been absorbed increasing the generated current. Since the size of the solar cell and the distance between the solar cell and the table, most of the radiation is dispersed onto the table, not contributing to higher current generation.

On CIGS' case, it was possible to perform a corner analysis of the solar panel and to estimate the panel's gallium concentration. To do so, three types of CIGS were selected: CIS, CIGS-45 and CGS. Analysing the respective responsivity, it was possible to check what wavelengths were and were not absorbed by the cell. For instance, the CGS solar

cell didn't absorb enough radiation to justify its I_{SC} value as much as CIGS-45, therefore through this corner analysis, it is possible to assume that the percentage of gallium of the solar panel at hand was between CIS and CIGS-45. But the best way to be absolutely sure of this should be through a more thorough and quantitative approach, which was what it was considered in the next chapter.

Finally, in chapter 6, a SEM analysis was in order. This could more easily determine how the layers within the cell were displayed as well as performing an EDS analysis, which allowed to study the constituents of the solar cell. Unfortunately, it was only possible to detect elements from the encapsulation layer, since at first the samples were prepared in the wrong arrangement, but at a second try it was possible to obtain cross-sectional SEM images from the solar cell, where all the layers could be observed.

CIGS solar cells achieved very good results throughout the experiments and during the simulations. However, silicon still proves to be an excellent PV technology, hence its market dominance. CIGS solar panels are definitely a technology to consider, specially in small applications where flexibility and versatility are key. Its market still has a lot of competition and its use of toxic chemicals are a huge barrier for it to enter the commercial world.

7.2 Future Work

For future studies and research in this topic, there is always room for improvement. The model that was created was mainly built from a semiconductor point of view, where it was possible to define the doping and the electrical properties of the material, but thanks to inclusion of the Multiphysics option of *COMSOL*, it was possible to generate a controlable incident radiation, where power and frequency could be user-defined.

The main upgrade that should be taken into consideration in future studies, is the design of a more realistic solar cell, given each cell is comprised of other elements that in real-life scenarios may affect its behaviour, such as the encapsulation materials and the other layers (in case of CIGS) that constitute the cell at hand.

Of course the upgrade from a 2D model to a 3D model will bring much close to reality results, since it is truly possible to recreate a solar cell in a laboratorial environment. However, new photovoltaic technologies should also include a study of the solar cell, under direct sunlight and outdoor exposure, since it can draw the physical limitations of these solar cells as well as the affect of environmental conditions on the devices under study.

Some of these new PV technologies are targeting the market of small applications, so that it will work as complementary energy system, many of it in the forms of flexible solar cells. This emerging technology, could also be submitted under stress bending tests in order to determine its limitations and affect to voltage and current produced.

Bibliography

[1] Bulent G. Akinoglu, Bilge Tuncel, and Viorel Badescu. Beyond 3rd generation solar cells and the full spectrum project. recent advances and new emerging solar cells. *Sustainable Energy Technologies and Assessments*, 46:101287, 2021.

[2] Mustafa Aljumaili, Ahmed Abdalkafor, and Mohammed Taha. Analysis of the hard and soft shading impact on photovoltaic module performance using solar module tester. *International Journal of Power Electronics and Drive Systems*, 10, Jun 2019.

[3] Tanvir Arfin and Arshiya Tarannum. Chapter 6 - engineered nanomaterials for industrial application: An overview. In Chaudhery Mustansar Hussain, editor, *Handbook of Nanomaterials for Industrial Applications*, Micro and Nano Technologies, pages 127–134. Elsevier, 2018.

[4] António Batista, Carlos F. Fernandes, Jorge Pereira, and José Paisana. Capítulo 1 - semicondutores. In LIDEL, editor, *Fundamentos da Eletrónica*, pages 1 – 91. 2012.

[5] Corsin Battaglia, Andres Cuevas, and Stefaan De Wolf. High-efficiency crystalline silicon solar cells: status and perspectives. *Energy Environ. Sci.*, 9:1552–1576, 2016.

[6] Aline Belusso. Análise do espetro de radiação solar. `https://docplayer.com.br/12993619-Titulo-analise-do-espectro-de-radiacao-solar-e-sua-importancia-no-correto-dimensionamento-de.html`. [Online; accessed 30-September-2021].

[7] Isabela C. B., Ricardo A. Marques Lameirinhas, João Paulo N. Torres, and Carlos A. F. Fernandes. Comparative study of the copper indium gallium selenide (cigs) solar cell with other solar technologies. *Sustainable Energy Fuels*, 5:2273–2283, 2021.

[8] H.C. Card and E.S. Yang. Electronic processes at grain boundaries in polycrystalline semiconductors under optical illumination. *IEEE Transactions on Electron Devices*, ED-24:397–402, 1977. ¡br /¿.

[9] Marco Casini. 10 - energy-generating glazing. In Marco Casini, editor, *Smart Buildings*, pages 327–353. Woodhead Publishing, 2016.

[10] Ilke Celik, Marina Lunardi, Austen Frederickson, and Richard Corkish. Sustainable end of life management of crystalline silicon and thin film solar photovoltaic waste: The impact of transportation. *Applied Sciences*, 10(16), 2020.

[11] Subhash Chander, A. Purohit, Anshu Sharma, Arvind, S.P. Nehra, and M.S. Dhaka. A study on photovoltaic parameters of mono-crystalline silicon solar cell with cell temperature. *Energy Reports*, 1:104–109, 2015.

[12] Lung-Chien Chen. Dye-sensitized solar cells with graphene electron extraction layer. In Sergei L. Pyshkin and John Ballato, editors, *Optoelectronics*, chapter 5. IntechOpen, Rijeka, 2015.

[13] Lung-Chien Chen, Cheng-Chiang Chen, and Bo-Shiang Tseng. Improvement of short-circuit current density in dye-sensitized solar cells using sputtered nanocolumnar tio¡sub¿¡b¿2¡/b¿¡/sub¿ compact layer. *Journal of Nanomaterials*, 2010:374052, Dec 2010.

[14] Afonso da Silva Ravasco, Joao Paulo N. Torres, and Ricardo Lameirinhas. Wearable photovoltaic applications as energy sources for everyday devices. *American Journal of Engineering and Applied Sciences*, 14(2):337–350, Jun. 2021.

[15] Samar Dabbabi, Tarek Ben Nasr, and Najoua Kamoun-Turki. Parameters optimization of cigs solar cell using 2d physical modeling. *Results in Physics*, 7:4020–4024, 2017.

[16] Rong Deng, Nathan L. Chang, Zi Ouyang, and Chee Mun Chong. A techno-economic review of silicon photovoltaic module recycling. *Renewable and Sustainable Energy Reviews*, 109:532 – 550, 2019.

[17] Jie Ding, Qiwei Han, Qian-Qing Ge, Ding-Jiang Xue, Jing-Yuan Ma, Bo-Ya Zhao, Yao-Xuan Chen, Jie Liu, David B. Mitzi, and Jin-Song Hu. Fully air-bladed high-efficiency perovskite photovoltaics. *Joule*, 3(2):402 – 416, 2019.

[18] Martin A. Green. Solar cell fill factors: General graph and empirical expressions. *Solid-State Electronics*, 24(8):788–789, 1981.

[19] Ali Imran, Jianliang Jiang, Deborah Eric, Muhammad Zahid, and Muhammad Yousaf. Parametric optimization of gaas pin solar cell. 08 2018.

[20] Nurnaeimah Jamalullail, Ili Salwani Mohamad, Mohd Natashah Norizan, N. Baharum, and Norsuria Mahmed. *Short review: Natural pigments photosensitizer for dye-sensitized solar cell (DSSC)*. Dec 2017.

[21] Nurnaeimah Jamalullail, Ili Salwani Mohamad, Mohd Natashah Norizan, and Norsuria Mahmed. Enhancement of energy conversion efficiency for dye sensitized solar cell using zinc oxide photoanode. *IOP Conference Series: Materials Science and Engineering*, 374:012048, 06 2018.

[22] Takuya Kato. Cu(in,ga)(se,s)2 solar cell research in solar frontier: Progress and current status. *Japanese Journal of Applied Physics*, 56, 2017.

[23] Young Yun Kim, Tae-Youl Yang, Riikka Suhonen, Marja Välimäki, Tiina Maaninen, Antti Kemppainen, Nam Joong Jeon, and Jangwon Seo. Gravure-printed flexible perovskite solar cells: Toward roll-to-roll manufacturing. *Advanced Science*, 6(7):1802094, 2019.

[24] Thomas Kirchartz and Uwe Rau. What makes a good solar cell? *Advanced Energy Materials*, 8(28):1703385, Oct 2018.

[25] Torben Klinkert. Comprehension and optimisation of the co-evaporation deposition of cu(in,ga)se2 absorber layers for very high efficiency thin film solar cells. 2015.

[26] A. Labouret, M. Villoz, J.L. Bal, and J. Hamand. *Solar Photovoltaic Energy*. Energy Engineering. Institution of Engineering and Technology, 2010.

[27] Jingwei Li, Yinhe Lin, Fanmao Wang, Jian Shi, Jifei Sun, Boyuan Ban, Guicheng Liu, and Jian Chen. Progress in recovery and recycling of kerf loss silicon waste in photovoltaic industry. *Separation and Purification Technology*, 254:117581, 2021.

[28] Christina Liedert, Lauri Rannaste, Annukka Kokkonen, Olli-Heikki Huttunen, Ralph Liedert, Jussi Hiltunen, and Leena Hakalahti. Roll-to-roll manufacturing of integrated immunodetection sensors. *ACS Sensors*, 5(7):2010–2017, 2020. PMID: 32469200.

[29] L. Lu, M.E. Ya'acob, M.S. Anuar, G. Chen, M.H. Othman, A. Noor Iskandar, and N. Roslan. Thermal analysis of a portable dssc mini greenhouse for botanical drugs cultivation. *Energy Reports*, 6:238–253, 2020.

[30] Marina Monteiro Lunardi, Juan Pablo Alvarez-Gaitan, José I. Bilbao, and Richard Corkish. A review of recycling processes for photovoltaic modules. In Beddiaf Zaidi, editor, *Solar Panels and Photovoltaic Materials*, chapter 2. IntechOpen, Rijeka, 2018.

[31] Marina Monteiro Lunardi, Juan Pablo Alvarez-Gaitan, and José I. Bilbaoand Richard Corkish. A review of recycling processes for photovoltaic modules, Feb 2018.

[32] Donald M. Mattox. Chapter 5 - thermal evaporation and deposition in vacuum. In Donald M. Mattox, editor, *The Foundations of Vacuum Coating Technology (Second Edition)*, pages 151–184. William Andrew Publishing, second edition edition, 2018.

[33] A.Niemegeers M.Burgelman. Calculation of cis and cdte module efficiencies. `https://users.elis.ugent.be/ELISgroups/solar/projects/scaps/MDS/Burgelman%20SolMat%201998.pdf`.

[34] Daniel de B. Mesquita, João Lucas de S. Silva, Hugo S. Moreira, Michelle Kitayama, and Marcelo G. Villalva. A review and analysis of technologies applied in pv modules. In *2019 IEEE PES Innovative Smart Grid Technologies Conference - Latin America (ISGT Latin America)*, pages 1–6, 2019.

[35] Seyed Roozbeh Nabavi, Felix Haase, Eelco Jansen, and Raimund Rolfes. Monte-carlo simulation of the cofiring process in polycrystalline silicon solar cells: Effects of material heterogeneity and thickness uncertainties. *Solar Energy Materials and Solar Cells*, 170:263–277, 2017.

[36] Preeti Nain and Arun Kumar. Theoretical evaluation of metal release potential of emerging third generation solar photovoltaics. *Solar Energy Materials and Solar Cells*, 227:111120, 2021.

[37] Kam Hoe Ong, Ramasamy Agileswari, Biancamaria Maniscalco, Panagiota Arnou, Chakrabarty Chandan Kumar, Jake W. Bowers, and Marayati Bte Marsadek. Review on substrate and molybdenum back contact in cigs thin film solar cell. *International Journal of Photoenergy*, 2018:9106269, Sep 2018.

[38] Sukanchan Palit and Chaudhery Mustansar Hussain. Chapter 1 - engineered nanomaterial for industrial use. In Chaudhery Mustansar Hussain, editor, *Handbook of Nanomaterials for Industrial Applications*, Micro and Nano Technologies, pages 3–12. Elsevier, 2018.

[39] Jae Park, Mowafak Al-Jassim, Seung Wook Shin, Jin Kim, and Tae Kim. Comprehensive characterization of cigs absorber layers grown by one-step sputtering process. *Ceramics International*, 45, Nov 2018.

[40] Janghoon Park, Keehyun Shin, and Lee Changwoo. Roll-to-roll coating technology and its applications: A review. *International Journal of Precision Engineering and Manufacturing*, 17:537–550, 04 2016.

[41] P. D. Paulson, R. W. Birkmire, and W. N. Shafarman. Optical characterization of cuin1xgaxse2 alloy thin films by spectroscopic ellipsometry. *Journal of Applied Physics*, 94(2):879–888, 2003.

[42] PVEducation. Series resistance model. `https://www.pveducation.org/pvcdrom/solar-cell-operation/series-resistance`. [Online; accessed 15-September-2021].

[43] PVEducation. Shunt resistance model. `https://www.pveducation.org/pvcdrom/solar-cell-operation/shunt-resistance`. [Online; accessed 16-September-2021].

[44] Tetsuo Soga. Chapter 1 - fundamentals of solar cell. In Tetsuo Soga, editor, *Nanostructured Materials for Solar Energy Conversion*, pages 3 – 43. Elsevier, Amsterdam, 2006.

[45] M.J. Theelen. Degradation of CIGS solar cells. `https://repository.tudelft.nl/islandora/object/uuid:2ce88658-a4c3-459f-afdc-00a5ac2c4ac4?collection=research`. [Online; accessed 16-September-2021].

[46] H S Ullal and B von Roedern. Thin film cigs and cdte photovoltaic technologies: Commercialization, critical issues, and applications; preprint. 5(5), 9 2007.

[47] Unknown. Lamp spectra. `https://guaix.fis.ucm.es/lamps_spectra`. [Online; accessed 16-September-2021].

[48] Yao Wu, Xin Yan, Wei Wei, Jinnan Zhang, Xia Zhang, and Xiaomin Ren. Optimization of gaas nanowire pin junction array solar cells by using algaas/gaas heterojunctions. *Nanoscale Research Letters*, 13(1):126, Apr 2018.

[49] Changqiao Yang, Suqin Li, Ruiming Yang, Jiaxing Bai, and Zijie Guo. Recovery of silicon powder from kerf loss slurry waste using superconducting high gradient magnetic separation technology. *Journal of Material Cycles and Waste Management*, 20(2):937–945, Apr 2018.

[50] Y. M. Yang, A. Yu, B. Hsu, W. C. Hsu, A. Yang, and C. W. Lan. Development of high-performance multicrystalline silicon for photovoltaic industry. *Progress in Photovoltaics: Research and Applications*, 23:340 – 351, Jan-03-2015 2015.

[51] Bekir Sami Yilbas, Abdullah Al-Sharafi, and Haider Ali. Chapter 3 - surfaces for self-cleaning. In Bekir Sami Yilbas, Abdullah Al-Sharafi, and Haider Ali, editors, *Self-Cleaning of Surfaces and Water Droplet Mobility*, pages 45 – 98. Elsevier, 2019.

[52] Min Yun, Seungil Cha, Han Kim, Seon Hee Seo, and Dong Lee. Monolithic-structured single-layered textile-based dye-sensitized solar cells. *Scientific Reports*, 6, 10 2016.

[53] Min Yun, Seungil Cha, Seon Seo, and Dong Lee. Highly flexible dye-sensitized solar cells produced by sewing textile electrodes on cloth. *Scientific reports*, 4:5322, 06 2014.

[54] Hugo Águas, Sanjay K. Ram, Andreia Araújo, Diana Gaspar, António Vicente, Sergej A. Filonovich, Elvira Fortunato, Rodrigo Martins, and Isabel Ferreira. Silicon thin film solar cells on commercial tiles. *Energy Environ. Sci.*, 4:4620–4632, 2011.